Journal of Structural Engineering. Submitted May 11, 2010; accepted February 10, 2011;
posted ahead of print February 12, 2011. doi:10.1061/(ASCE)ST.1943-541X.0000392

Retracted: A Constitutive Model of Circular Steel Tubes and Its Applications in Analysis of Space Structures

F. Fan[1]; G. B. Nie[2]; and X. D. Zhi[3]

Abstract: Developed rapidly in the recent thirty years, space structures in the form of reticulated shells are widely used in all kinds of large-scale public buildings. The performance of the tubular components of the structures is significantly influenced by large deformation and obvious material plasticity encountered in severe earthquakes. The material behavior needs to be considered in the constitutive model. Tests of fifty circular steel tubes were thus conducted under cyclic axial and horizontal loads to derive the rational constitutive model with consideration of material damage accumulation. The results show that the degree of damage depends on parameters of the tubes and the loading history. Finite element model simulating the performance of the steel tubes was then developed incorporating a user-defined material sub-routine UMAT encoded with ABAQUS. A generalized constitutive model of circular steel tubes considering damage accumulation was derived by means of the least square method fitting between numerical simulation and experimental results. Using the finite element model, responses of reticulated shells with different parameters under severe earthquakes have been investigated and the characteristic responses at structural failure have been discussed as well. It was found out that the damage accumulation decreases the structural failure load obviously, which needs to be considered in the analysis and design of the structures.

Keywords: Circular Steel Tube; Damage Accumulation; Hysteretic Behavior; Constitutive Model; Finite Element.

Introduction

The space structures in the form of reticulated shells are wildly used in sport gymnasia, railway stations, airport terminal buildings, conference centers, exhibition halls and some other large-scale public buildings. Collapse of such structures due to earthquakes can cause tremendous loss of lives and properties. How to guarantee the safety of lives and reduce the loss of properties subjected to severe earthquakes has drawn much attention from the research community worldwide. The space structures usually present large deformation and obvious material plasticity under severe earthquakes which indicate strength failure of the structure. Thus, the performance of the tubular components of the structures under earthquakes is of great importance for preventing failure of structure. The theoretical study of the earthquake performance of tubes is complicated and requires consideration of material behavior in the constitutive model. Therefore, it is necessary to develop a rational material damage model to evaluate the damage accumulation in the material constitutive model. Such a damage model was studied by many researchers from different areas. Hearn and Testa (1991) described the damage from the decrease of the cross-sectional area of specimen. Powell and Allahabadi (1988) introduced the damage model with deformation of specimen. The specific model composed of linear combination of deformation and energy was presented by Park et al (1985), and this model was regarded as a breakthrough because deformation and energy were treated as the cause of damage. Based on Park's model, Kumar et al (1996) and Gao et al (1998) investigated many experiments conducted on hollow steel box columns and developed a damage model to evaluate the damage accumulation. Dong et al (1999) and Shen et al (2002) developed a damage model based on cyclic loading tests on I-sectioned steel columns. Also, the corresponding finite element program using the model to analyse high-rise steel structures was developed. However, the above mentioned researchers focused their attention on the

[1] Research Student, School of Civil Engineering, Harbin Institute of Technology, P.O. Box 2619, Haihe Rd., Nangang District, Harbin 150090, P. R. China. E-mail: nieguibo0323@163.com

[2] Professor, School of Civil Engineering, Harbin Institute of Technology, P.O. Box 2619, Haihe Rd., Nangang District, Harbin 150090, P. R. China.

[3] Professor, School of Civil Engineering, Harbin Institute of Technology, P.O. Box 2619, Haihe Rd., Nangang District, Harbin 150090, P. R. China.

Journal of Structural Engineering. Submitted May 11, 2010; accepted February 10, 2011;
posted ahead of print February 12, 2011. doi:10.1061/(ASCE)ST.1943-541X.0000392

components only subjected to cyclic horizontal loads, with the axial compression being constant, which are appropriate for high-rise and some other structures because these structures are mainly subjected to horizontal earthquake loads. For space structures, the vertical earthquake loads are as important as horizontal earthquake loads. The behavior of space structures under three-direction earthquake loads is more complex, the constitutive model needs to take this complexity into account. In view of these complications, experiments are a reasonable way to develop the constitutive model involving material damage. So far there are hardly any published studies on the material behavior under three-direction cyclic loads.

In this paper, experiments were conducted on fifty circular steel tubes, using a constant or cyclic axial load and different horizontal loading schemes. The hysteretic energy dissipation capacity of specimens with different slenderness ratios and different loading schemes was investigated; then, a user-defined material sub-routine UMAT was encoded incorporating ABAQUS to perform numerical simulation of the experiment. Furthermore, a generalized constitutive model of circular steel tubes considering damage accumulation was developed using the least squares method. Comparison between numerical simulation and experimental results shows close agreement between the two, which proves not only the constitutive model is accurate but also the finite element model is applicable to numerical analysis. Finally, using the constitutive model, responses of reticulated shells with different parameters under severe earthquakes were investigated and the characteristic responses at structural failure have been discussed. Using the method presented in this paper, the effect of the damage accumulation on the performance of the space structures can be accurately quantified.

Outline of Experiments

Experiment Setup and the Specimens

Circular steel tubes with a height of 900mm, 1200mm and 1500mm and a cross-section of Φ76X5mm, Φ114X5mm and Φ140X5mm, respectively, were chosen to cover different slenderness ratios applicable in engineering practice. All the specimens as shown in Table 1 were tested as cantilevered tubes. To verify the stability of the experiment device and data acquisition system, two groups of specimens with specimens number S-06 and S-12 were completed. The first group included three specimens and the second group included two specimens with the corresponding load mode 1 and 2. These five specimens also added to the total specimens. So the total of the specimens are fifty and the details in table 1 are forty-five. Junction plates were welded to the top of specimen to provide the rotations in the horizontal planes, as shown in Fig.1a. The top plate and the bottom plate with pre-drilled circular holes to accommodate bolts were welded at the two sides of specimen. To reinforce the stiffness and stability of the experiment setup, the bottom plate at the bottom of specimen was connected to the steel box using high strength bolts. The reaction frames were specially designed with sufficient stiffness. Junction plates were also welded in different height of the reaction frame to suit different heights of the specimens. The steel beams linking the steel box and the reaction frames formed a self-balancing system, as shown in Fig.1b and c.

Since the specimen deflects in two directions under two-direction horizontal loading, the specimen and the jack as well as the jack and the reaction frame were connected via a full hinge to provide sufficient rotations in the two directions. A LVDT and a load cells were applied to the top of specimen along the two mutually perpendicular directions, respectively, as shown in Fig.2a. It is vital that the specimen is applied with an axial load at the top while the top end is kept free. The experiment setup was designed as follows to achieve this. Fig.2b shows part of the setup through which either the tension or the compression can be applied. While Fig.2c shows the scheme to apply the compression load to the specimen. A steel rod with a diameter of 45mm that can withstand both tension and compression went through the hollow tube. Then a steel ball was added to the rod via threads to stop the movement of the rod once the rod is in tension. An upward load

Journal of Structural Engineering. Submitted May 11, 2010; accepted February 10, 2011;
posted ahead of print February 12, 2011. doi:10.1061/(ASCE)ST.1943-541X.0000392

was applied to the fixed plate by the jack. The fixed plate was connected to the rod also via threads. Thus the specimen was in compression due to the reaction of the jack, while the rod is in tension. Fig.2d shows the scheme to apply the tension load to the specimen. An upward load was also applied to the free-movement plate by the jack. The plate was then stopped by the nuts on each of the four tension bars that were linked to the specimen, and the tension load was thus applied to the specimen. Now the central rod is in compression due to the reaction of the jack. The axial load was controlled by the reading from the load cell, while the horizontal load in both directions was controlled by the required displacement from the LVDT.

To investigate the damage effects of load history, nine series of tests were conducted, each with identical specimens of circular steel tubes but with different loading schemes. Of the loading schemes, load schemes 1 to 5 are constant axial load with the amplitude about sixty percent of its tensile strength of the cross-section and the other five load schemes are cyclic axial load. For each of the nine series, the cyclic loads in the horizontal direction are the same. The numbers of the five load schemes with constant axial load are Load scheme 1 to Load scheme 5 and the numbers of the other five load schemes with cyclic axial load are Load scheme 6 to Load scheme 10. This paper only gives the five load schemes with cyclic axial load, as shown in Fig.3. Load scheme 6 simulates earthquake action with the identical period and identical phase in the two horizontal directions by keeping the horizontal thrust identical; load scheme 7 applies constant load in horizontal direction of x and cyclic load in the direction of y. The horizontal load in x direction is then increased gradually until the specimen fails; load scheme 8 applies constant load in the horizontal direction of x and then the horizontal load in y direction is increased or decreased alternatively until the specimen fails; load scheme 9 simulates earthquake action in the two horizontal directions with the same period but different phases; load scheme 10 simulates earthquake action in the two horizontal directions with different periods and phases. In this paper, two-direction means the axial load is constant and three-direction means the axial load is cyclic.

Test Observations

The damage accumulation of a specimen depends on its response under loads that is function of its loading history. Failure of all specimens involved is local buckling at the bottom of specimen. The hysteretic curves of only one group of specimens, S-21 to S-25, are given in Fig.4.

Take Specimen S-23 under two-direction as an example, the hysteretic load-displacement curves got from experiment are shown in Fig.5. The abscissa stands for the displacement of the cantilevered top end of specimen and the ordinate stands for the horizon load applied to the top end. Fig.5. shows that the coverage area of the hysteretic curve is almost zero when the specimen is loaded under cyclic horizontal displacement within the elastic range (the loading displacement is approximately between -4mm and 4mm). The energy dissipation is approximately zero because the strain energy is elastic. The residual deformation still exists when the load decreases to zero during the procedure of cyclic loading. For each half-cycle, the higher the amplitude of load is, the larger the residual deformation becomes. Buckling of tube wall becomes visible at the 9th half-circle in test and the peak load starts deteriorate with a value of displacement of 60mm, which indicates that the specimen has good energy dissipation capacity; the peak load decreases faster after the displacement is over 60mm. At the 10th half-circle with a value of displacement of 80mm, the effect of buckling becomes considerable. Meanwhile, though with a slenderness ratio of 120, overall buckling of the tube as Euler rod did not happen in the test. To understand the complexity of the spatial hysteretic behavior to the load histories, Specimen S-28 as also shown in Fig.5 is compared with S-23. Both of them are the same in cyclic horizontal load but different in axial load. The results of S-28 under three-direction loading show that the responses are more complex than that of S-23. The load in each half-cycle is more different to control and the load in one direction is easily affected by the load in the other direction when conducting the

Journal of Structural Engineering. Submitted May 11, 2010; accepted February 10, 2011;
posted ahead of print February 12, 2011. doi:10.1061/(ASCE)ST.1943-541X.0000392

test. Even with the same horizontal load, the smoothness of the hysteretic curve in three-direction test is not ideal than that of two-direction test. All mentioned above indicates that the complexity of the response is related to the complexity of loading.

Analysis of the Experimental Results

It is important to eliminate the experiment errors since the experiment results will be inevitably affected by the accuracy of the experiment setup and some other factors. Take Specimen S-23 as an example, there are two experiment errors explained as follows:

(1) The accuracy of experiment results is susceptible to the rigid body rotation of the steel box at the bottom of specimen as shown in Fig.6. The vertical displacements from the four LVDT's as shown in Fig.6a are recorded. Take Y direction as an example, the centre point displacement between LVDT 1 and LVDT 4 is obtained from the averaged displacement of them. Similarly, the displacement between the LVDT 2 and the LVDT 3 is obtained. The top end displacement of the specimen by rotation of the steel box can be revised by the linear relationship, as shown in Fig.6a. The displacement error is constant if the specimen works in the elastic range. When the specimen undergoes nonlinear behavior, especially when buckling happens, the displacement error caused by the rigid body rotation of the steel box becomes more considerable. The comparison of the revised curves with the un-revised curves is shown in Fig.6b and c, which shows that the maximum displacement error caused by the rigid body rotation of the steel box can be up to 10%.

(2) As shown in Fig.7a, the load cell at the loading point and the LVDT at the top plate are not in the same level. The load and displacement in curves obtained from test should be from the same level. Therefore, the displacement at the top is needed to adjust to the loading point to eliminate this experiment error. Due to the small vertical distance between the load cell and the LVDT, the displacement error can be considered as proportional to the displacement. The comparison of the revised curves and unrevised curves is shown in Fig.7b, which indicates that the displacement error caused by this factor can be up to 18% at the ultimate load and with a value of displacement of 80mm.

Damage Index and the Constitutive Model

The material damage includes plasticity development, initiation and development of small cracks. Due to such micro-damage, the performance of the material will be deteriorated. Actions of load, temperature, chemicals and the environment can cause micro-and macro-flaws inside the material. Under these circumstances the material is considered in a damaged state. The degree of material damage is expressed by the damage index D. The characteristics of D can be described as follows:

1. The value of D ranges between 0 and 1. D=0 means the material is without damage, and D=1 means complete failure of material.
2. Damage index D is a monotonically increasing function, which indicates that the development of damage is non-reversible.

Some researchers pay their attention to damage from an energy point of view. Satish and Usami (1994) presented Eq. (1) to express the degree of damage.

$$D = \sum_{i=1}^{n} \beta_i \left(\frac{E_i}{E_u}\right)^c \quad (1)$$

where n=number of half-cycles which induce plastic strain; β_i =weight value of each half-cycle; E_i = the hysteretic energy increment of the ith half-cycle; E_u =the maximum energy dissipation under monotonic loading; c=non-negative parametric constant. To emphasize the significance of the half-cycle when the maximum plastic deformation happens and the value of D is 1 at the monotonic loading, the weight value of

Journal of Structural Engineering. Submitted May 11, 2010; accepted February 10, 2011;
posted ahead of print February 12, 2011. doi:10.1061/(ASCE)ST.1943-541X.0000392

this cycle is $1-\beta$. Eq. (1) can thus be rewritten into

$$D=(1-\beta)\frac{E_m}{E_u}+\sum_{i=1}^{n}\beta_i\frac{E_i}{E_u} \tag{2}$$

The damage happens when the material develops the plasticity, plastic strain is adopted to measure the degree of damage. The failure damage index is thus developed into Eq. (3)

$$D=(1-\beta)\frac{\varepsilon_m^p}{\varepsilon_u^p}+\beta\sum_{i=1}^{N}\frac{\varepsilon_i^p}{\varepsilon_u^p} \tag{3}$$

where ε_m^p = the largest plastic strain in all half-cycles; ε_i^p = the plastic strain of ith half-cycle; ε_u^p = the ultimate plastic strain of steel under monotonic loading. At the same time, the elastic modulus and yield stress of material corresponding to damage index D are expressed, respectively, as

$$E_D=(1-\xi_1 D)E \tag{4}$$

$$\sigma_D=(1-\xi_2 D)\sigma_S \tag{5}$$

where E and E_D are the elastic modulus corresponding to D=0 and D, respectively, σ_s is the initial yield stress when D=0; and σ_D is the yield stress with respect to D. ξ_1 and ξ_2 are two material parameters. Eqs. (3) to (5) form a set of equations to describe the constitutive relationships considering material damage accumulation. The performance of the material can be described accurately by this set of equations. The aim of this paper is to evaluate the parameters like ξ_1, ξ_2 and β in the equations. These parameters are determined by using the numerical method to simulate the whole experiment process.

To satisfy the specific requirement of this study, a user-defined sub-routine UMAT was developed to include the material constitutive model developed based on the test. The core of the subroutine is to update the stresses, strains, and material properties for subsequent load increments. The description of the material in the subroutine adopts Von-Mises rule and J_2 plastic flow theory. The process of UMAT is provided by a flowchart, as shown in Fig.8. Inputting any given displacement obtained in the test, the program incorporated with the UMAT will output corresponding load of specimen. Then the numerical curve got from the ABAQUS can be compared with experiment curve by putting them into one map. The user can get different hysteretic curves with different β, ξ_1 and ξ_2.The value of β, ξ_1 and ξ_2 is so determined when the two curves match best at apex points of the hysteretic curves. Fig.9 shows the curves of Specimen S-12 as an example, the two curves match best when β =0.019 , ξ_1 =0.331 , ξ_2 =0.059. Using the above-mentioned principle, the parameters in the material model of all other specimens are obtained and are listed in Table 2. Finally, using the data in Table 2, a generalized constitutive equation of circular steel tubes considering damage accumulation was developed by the least squares fitting method with β =0.0268 , ξ_1 =0.404 , ξ_2 =0.063.

Validation of the Constitutive Model

To validate the generalized constitutive model, all the specimens were re-simulated. Take Specimens S-21 and S-27 as examples, the hysteretic load-displacement curves obtained from the experiment and the corresponding curves from the numerical simulation with ABAQUS, are shown in Fig.10. The figure indicates that the numerical curves are in good agreement with the experiment curves. This proves that not only the constitutive model of circular steel tubes with damage accumulation is accurate but also the

Journal of Structural Engineering. Submitted May 11, 2010; accepted February 10, 2011;
posted ahead of print February 12, 2011. doi:10.1061/(ASCE)ST.1943-541X.0000392

user-defined sub-routine UMAT is applicable to numerical analysis.

Analysis of the earthquake performance of reticulated shells considering the damage accumulation

A parametric study was conducted on single-layer reticulated spherical shells and cylindrical shells subjected to earthquake loading. The reticulated shells are shown in Fig.11 and the parameters for analysis are listed in Table 3. The single-layer reticulated spherical shells are of Kiewitt 8 type and the boundary conditions are pinned joints along the base; the single-layer reticulated cylindrical shells are of three-dimensional latticed mesh with the supports along the longitudinal direction hinged and the supports along the arch direction restrained only in vertical direction. The Raleigh damping with a damping ratio of 0.02 is adopted. The reticulated shells begin to present some damage when the earthquake load intensity reaches certain degree, and this damage can be reflected using the user-defined sub-routine UMAT with the Damage Index D included in the material constitutive model developed.

The nonlinear analysis to investigate the structural responses under different earthquake load intensities was conducted. In order to simulate responses of the reticulated shells under severe earthquakes, the FE models using beam elements divided into three segments, beam 31 (Zhi 2006), were developed. There are 8 integration points over the cross-section, as shown in Fig.12. The material represented by an integration point is defined as failure when the damage index D=1. Symbol nP (n=1, 2, 3…8) indicates that material at n integration points fails, as shown in Fig.12. The dynamic load is expressed in terms of the acceleration gal (cm/s^2).

Take reticulated spherical shell (L=60m , f/L=1/3 , Mass destiny=60kg, Taft(1952)) as an example, as shown in Fig.11a. Firstly, for the purpose of comparison, the perfect elasto-plastic material model is adopted to conduct the analysis. Then analysis considering the damage accumulation expressed with Eqs. (3) to (5), was conducted. All other parameters are the same in the two cases. The analytical results of the characteristic responses of the structure with and without considering damage accumulation are shown in Fig.13. Without considering the damage accumulation, plasticity begins to develop when the magnitude of earthquake load reaches 450gal. With increase of the earthquake magnitude, the plasticity of the structure develops gradually and performance of the structure deteriorates; the maximum node displacement increases with earthquake load, and 1300gal can be identified as the failure load, since the vibration becomes divergent when the load exceeds this value. At the failure, the maximum node displacement is 0.2m, the 1p yielded member ratios is 62.1% and the 8p yielded member ratios is 23.9%; at the same time, 79 members of structure encounter full failure, among them, 17 members failed due to tension and the mean strain reaches 1.1×10^{-3}, which indicates that the structure has been in deeply plasticity destruction of material.

When considering the damage accumulation, though the responses of the above mentioned spherical shell subjected to the same earthquake load show little differences in the plasticity development and the number of yielded members from the case without considering, yet the failure load is 1100gal (Fig.13b), obviously lower than 1300 gal. Therefore, to use the perfect elasto-plastic material model to get the analytical results is not sufficient. The effect of material damage accumulation can not be ignored when conducting earthquake performance analysis of the reticulated shells.

The parametric study of the reticulated spherical and cylindrical shells was completed to evaluate the effect of the constitutive model with damage accumulation. The 1p and 8p yielded member ratios of spherical shells and the effect on the failure load in cylindrical shells are shown in Fig.14a and b, respectively. Fig.14a shows that the member ratio of material yield are more than 60%, in all the cases, at least 20% of members are full-section yielding, which indicates that the extent of plasticity development is serious. There is no

Journal of Structural Engineering. Submitted May 11, 2010; accepted February 10, 2011;
posted ahead of print February 12, 2011. doi:10.1061/(ASCE)ST.1943-541X.0000392

significant difference in plasticity development of the spherical shells at failure between the cases with and without considering damage accumulation, but the failure load with damage accumulation decreases significantly. In some cases, the decrease is as much as 20%. The load is one of the most important issues in engineering practice, accurate prediction of it by considering the damage accumulation is of great significance.

Conclusions

Through the investigation of the spatial hysteretic behavior of the circular steel tubes under cyclic loading and the responses of the reticulated shells with different parameters under severe earthquake, the following conclusions can be drawn.

The experimental setup applicable for three-direction loading was designed to cover different slenderness ratios and different load schemes. Experimental results prove that the experiment setup is stable.

The user-defined sub-routine UMAT in ABAQUS considering the effect of the damage accumulation was encoded and the hysteretic curves of specimens were calibrated. Then the generalized constitutive equation of circular steel tubes considering the damage accumulation was developed by the least square fitting method with the specimens between experiment results and numerical simulation.

The results from numerical simulation are in good agreement with the experiments. This proves that not only the constitutive equation is accurate but also the FE model incorporating UMAT is applicable to dynamically nonlinear analysis of the structures subjected to earthquake load.

With increase of plasticity, the difference between the curves with and without considering damage accumulation becomes more and more obvious, which obviously reduces the failure load of the structure. Considering the damage accumulation is of great significance since the load is one of the most important issues in engineering practice.

Notation

The following symbols are used in this paper:

c=none-negative parametric constants;

d= specimen diameter;

D=the damage index;

L=specimen length;

n=number of half-cycles;

t= wall thickness of specimen;

θ=the angle of the rotation of the steel box;

λ = slenderness ratio;

β_i=weight value of each half-cycle;

E_i= the hysteretic energy increment of i half-cycle;

E_u=the max hysteretic energy under monotonic loading;

E= Young's modulus without damage;

E_D= Young's modulus with damage;

σ_s= the yield strength without damage;

σ_D= the yield strength with damage;

ξ_1= parameters determined by the experiment;

Journal of Structural Engineering. Submitted May 11, 2010; accepted February 10, 2011;
posted ahead of print February 12, 2011. doi:10.1061/(ASCE)ST.1943-541X.0000392

ξ_2= parameters determined by the experiment;

ε_m^p= the maximum plastic strain of steel under load;

ε_i^p = the plastic strain of steel of i half-cycle;

ε_u^p = the limit plastic strain of steel under monotonic loading.

References

ABAQUS theory manual Version 6.1. (2000a). Hibbitt, Karlsson & Sorensen, Inc., Pawtucket, R.I.

ABAQUS user's manual Version 6.1. (2000a). Hibbitt, Karlsson & Sorensen, Inc., Pawtucket, R.I.

Dong, B., Shen Z. Y., and Sun, F, F. (1999). "Simulation of spatial hysteretic behavior of steel columns considering effects of damage accumulation." Journal of Tongji University., 27(1), 11~15.

Gao, S. B., Usami, T., and GE, H. B. (1998). "Ductility evaluation of steel bridge piers with tubes sections." J. Struct. Mech., ASCE, 124(3),260-267.

Hearn G., Testa R. B. (1991). "Modal Analysis for Damage Detection in Structures." J. Struct. Engre., ASCE, 117(10):3042~3063.

Powell G. H., and Allchabadi, R. (1988) "Seismic Damage Prediction by Deterministic Methods: Concept and Procedures." Earthquake Engineering and Structural Dynamics,16(5),719~734

Park, Y. J., and Ang, A. H. S. (1985). "Mechanistic seismic damage model for reinforced concrete." J. Struct. Engre., ASCE,111(4),722-739.

Park, Y. J., Ang, A. H. E., and Wen, Y. W. (1985) "Seismic damage analysis of reinforced concrete buildings." J. Struct. Engre., ASCE,111(4),740-757.

Kumar, S., and Usami, T. (1996). "Damage evaluation in Steel box columns by cyclic loading tests." J. Struct. Engre., ASCE, 122(6),626-634.

Shen, Z. Y., and Shen, S. (2002). "Earthquakes analysis of tall steel structures with damage cumulation and fracture effects." Journal of Tongji University., 30(4):393~398.

Kumar, S., and Usami, T. (1994). "A note on the evaluation of damage in steel structures under cyclic loading." J. Struct. Engre., Tokyo, Japan, 40A, 177-188.

ZHI Xu-dong. (2006). "Failure mechanism of reticulated shells under severe earthquakes motion. " Dissertation for the Degree of Doctor, Harbin Institute of Technology.

Journal of Structural Engineering. Submitted May 11, 2010; accepted February 10, 2011;
posted ahead of print February 12, 2011. doi:10.1061/(ASCE)ST.1943-541X.0000392

Table 1 Details and designation of specimen

specimen	Height (mm)	Outer diameter (mm)	Load scheme	λ	specimen	Length (mm)	Outer diameter (mm)	Load scheme	λ	specimen	Height (mm)	Outer diameter (mm)	Load scheme	λ
S-01	900	140	1	38	S-16	1200	140	1	50	S-31	1200	76	6	95
S-02			2		S-17			2		S-32			7	
S-03			3		S-18			3		S-33			8	
S-04			4		S-19			4		S-34			9	
S-05			5		S-20			5		S-35			10	
S-06(4)	900	114	1	47	S-21	1500	140	1	63	S-36	1500	114	6	78
S-07			2		S-22			2		S-37			7	
S-08			3		S-23			3		S-38			8	
S-09			4		S-24			4		S-39			9	
S-10			5		S-25			5		S-40			10	
S-11	900	76	1	72	S-26	1200	114	6	62	S-41	1500	76	6	119
S-12(3)			2		S-27			7		S-42			7	
S-13			3		S-28			8		S-43			8	
S-14			4		S-29			9		S-44			9	
S-15			5		S-30			10		S-45			10	

Journal of Structural Engineering. Submitted May 11, 2010; accepted February 10, 2011;
posted ahead of print February 12, 2011. doi:10.1061/(ASCE)ST.1943-541X.0000392

Table 2 value of parameters in damage index D of circular steel tubes

Number	β	ξ_1	ξ_2	Number	β	ξ_1	ξ_2	Number	β	ξ_1	ξ_2
S-01	0.017	0.401	0.061	S-13	0.028	0.382	0.057	S-30	0.035	0.448	0.073
S-02	0.019	0.404	0.062	S-14	0.017	0.321	0.057	S-31	0.030	0.407	0.061
S-03	0.022	0.411	0.06	S-15	0.016	0.335	0.058	S-32	0.031	0.417	0.061
S-04	0.032	0.441	0.063	S-16	0.015	0.321	0.061	S-33	0.032	0.436	0.070
S-05	0.017	0.401	0.061	S-17	0.033	0.421	0.063	S-34	0.034	0.418	0.071
S-06-1	0.034	0.441	0.039	S-18	0.034	0.421	0.063	S-35	0.033	0.406	0.069
S-06-2	0.034	0.436	0.04	S-19	0.026	0.421	0.063	S-36	0.030	0.411	0.069
S-06-3	0.034	0.436	0.04	S-20	0.015	0.401	0.061	S-37	0.031	0.423	0.071
S-06-4	0.034	0.411	0.044	S-21	0.023	0.422	0.062	S-38	0.032	0.415	0.073
S-07	0.014	0.303	0.067	S-22	0.015	0.411	0.063	S-39	0.033	0.427	0.074
S-08	0.034	0.432	0.05	S-23	0.028	0.421	0.063	S-40	0.034	0.427	0.075
S-09	0.017	0.398	0.062	S-24	0.022	0.421	0.063	S-41	0.030	0.398	0.069
S-10	0.016	0.401	0.061	S-25	0.014	0.324	0.059	S-42	0.031	0.409	0.071
S-11	0.027	0.381	0.058	S-26	0.032	0.442	0.072	S-43	0.032	0.419	0.072
S-12-1	0.021	0.341	0.061	S-27	0.033	0.423	0.072	S-44	0.033	0.428	0.073
S-12-2	0.018	0.321	0.058	S-28	0.033	0.433	0.070	S-45	0.034	0.437	0.074
S-12-3	0.019	0.331	0.059	S-29	0.034	0.445	0.075				

Journal of Structural Engineering. Submitted May 11, 2010; accepted February 10, 2011;
posted ahead of print February 12, 2011. doi:10.1061/(ASCE)ST.1943-541X.0000392

Table 3 Parameters of reticulated shells for analysis

	The spherical shells	The cylindrical shells
Earthquakes input	Taft(1952); El-Centro(1940)	Taft(1952)
Rise to span ratio	1/3, 1/5, 1/7	N/A
Roof mass (kg/m^2)	60, 120, 180	
Length to width ratio (*L/B*)	N/A	1.4, 1.8
Rise to width ratio (*f/B*)	N/A	1/2, 1/3, 1/5

Journal of Structural Engineering. Submitted May 11, 2010; accepted February 10, 2011;
posted ahead of print February 12, 2011. doi:10.1061/(ASCE)ST.1943-541X.0000392

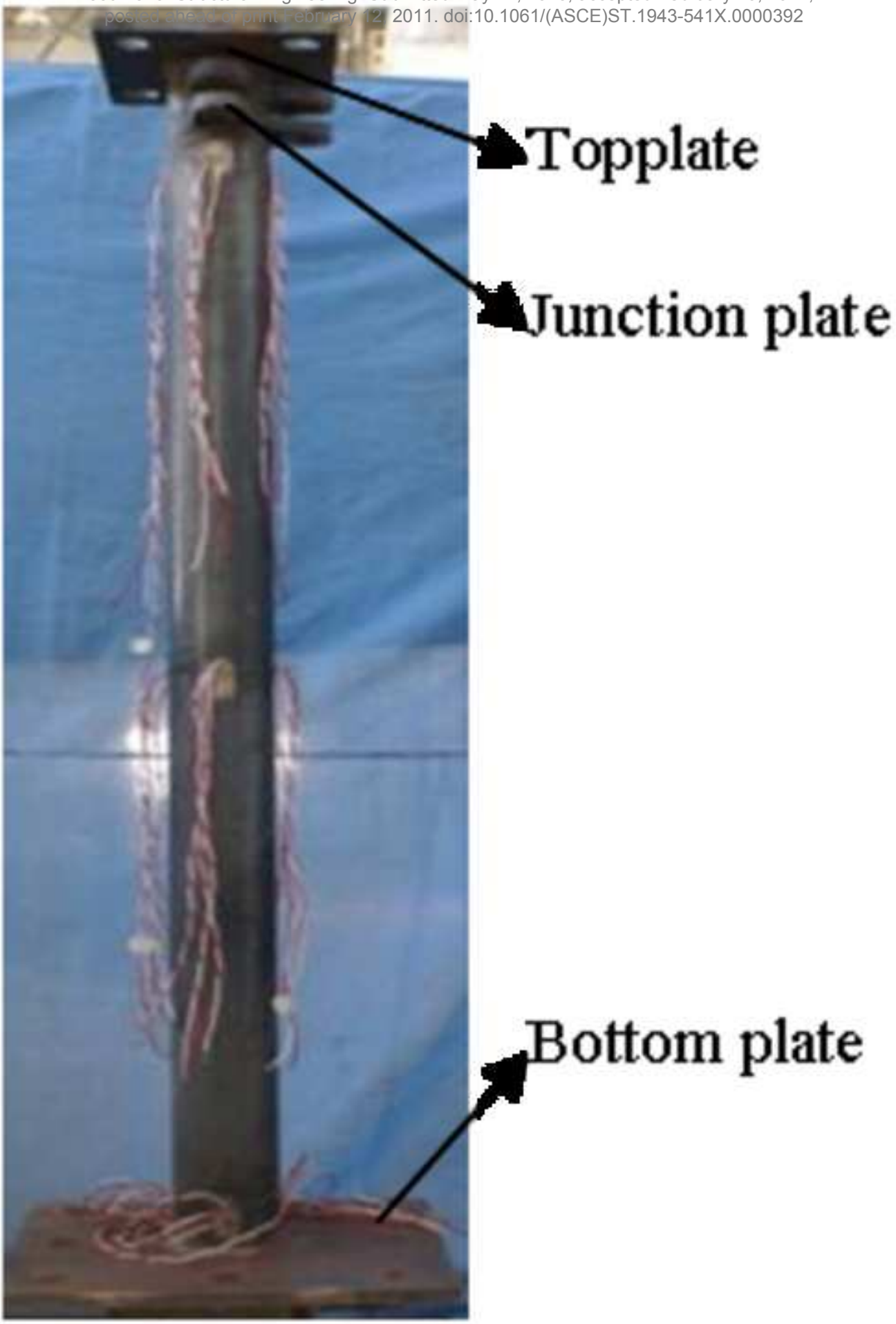

Journal of Structural Engineering. Submitted May 11, 2010; accepted February 10, 2011;
posted ahead of print February 12, 2011. doi:10.1061/(ASCE)ST.1943-541X.0000392

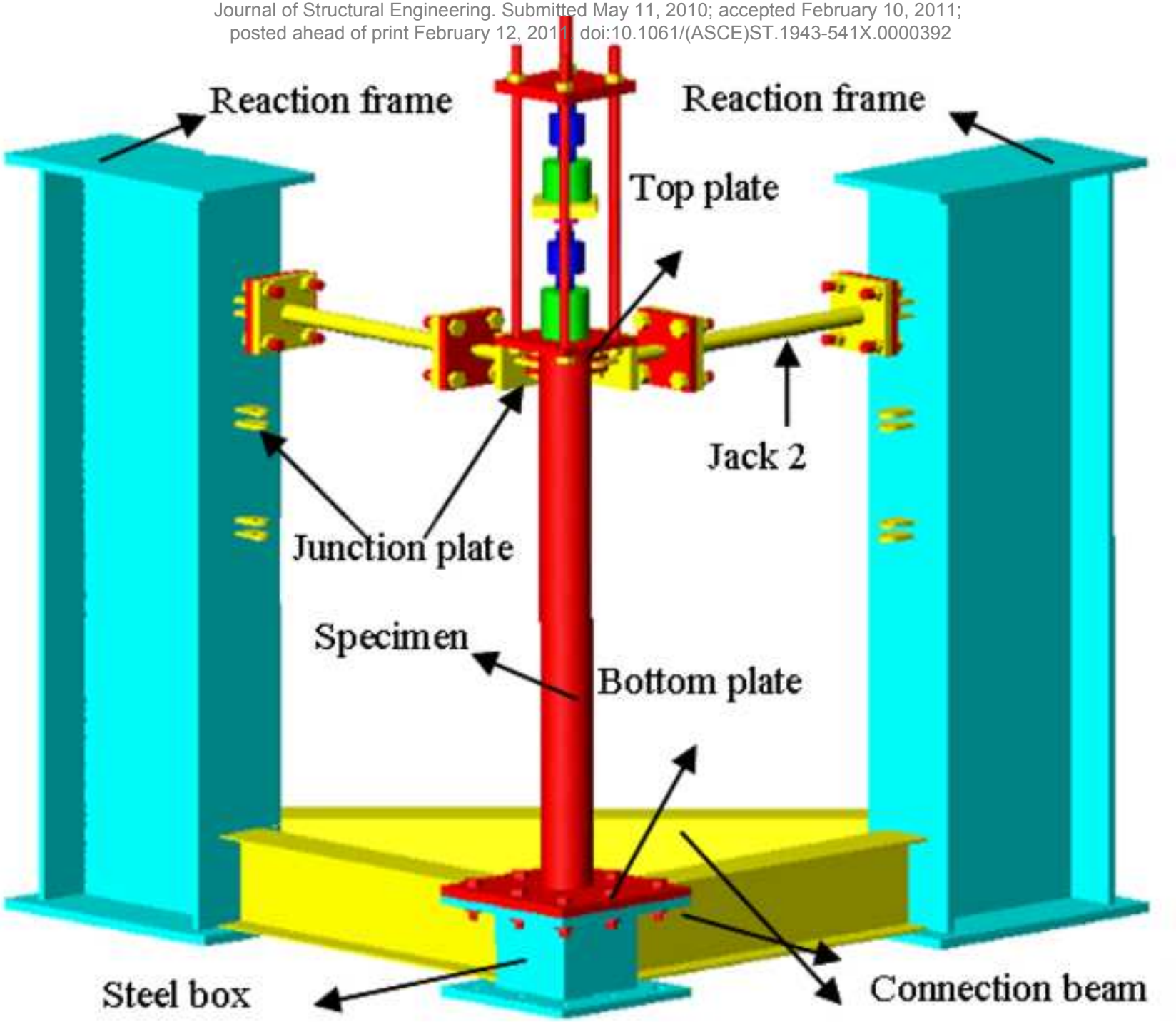

Journal of Structural Engineering. Submitted May 11, 2010; accepted February 10, 2011;
posted ahead of print February 12, 2011. doi:10.1061/(ASCE)ST.1943-541X.0000392

Journal of Structural Engineering. Submitted May 11, 2010; accepted February 10, 2011;
posted ahead of print February 12, 2011. doi:10.1061/(ASCE)ST.1943-541X.0000392

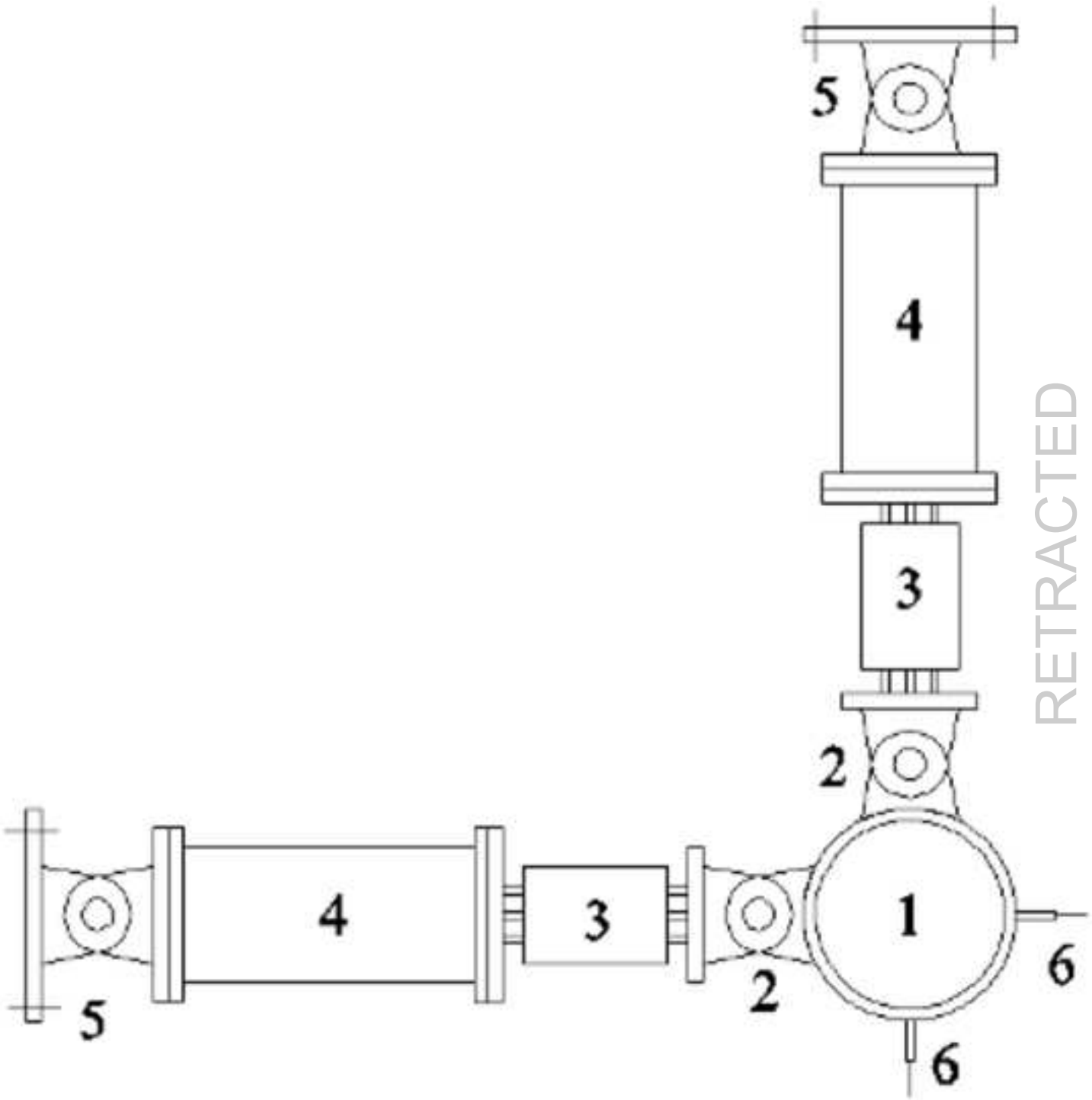

Journal of Structural Engineering. Submitted May 11, 2010; accepted February 10, 2011;
posted ahead of print February 12, 2011. doi:10.1061/(ASCE)ST.1943-541X.0000392

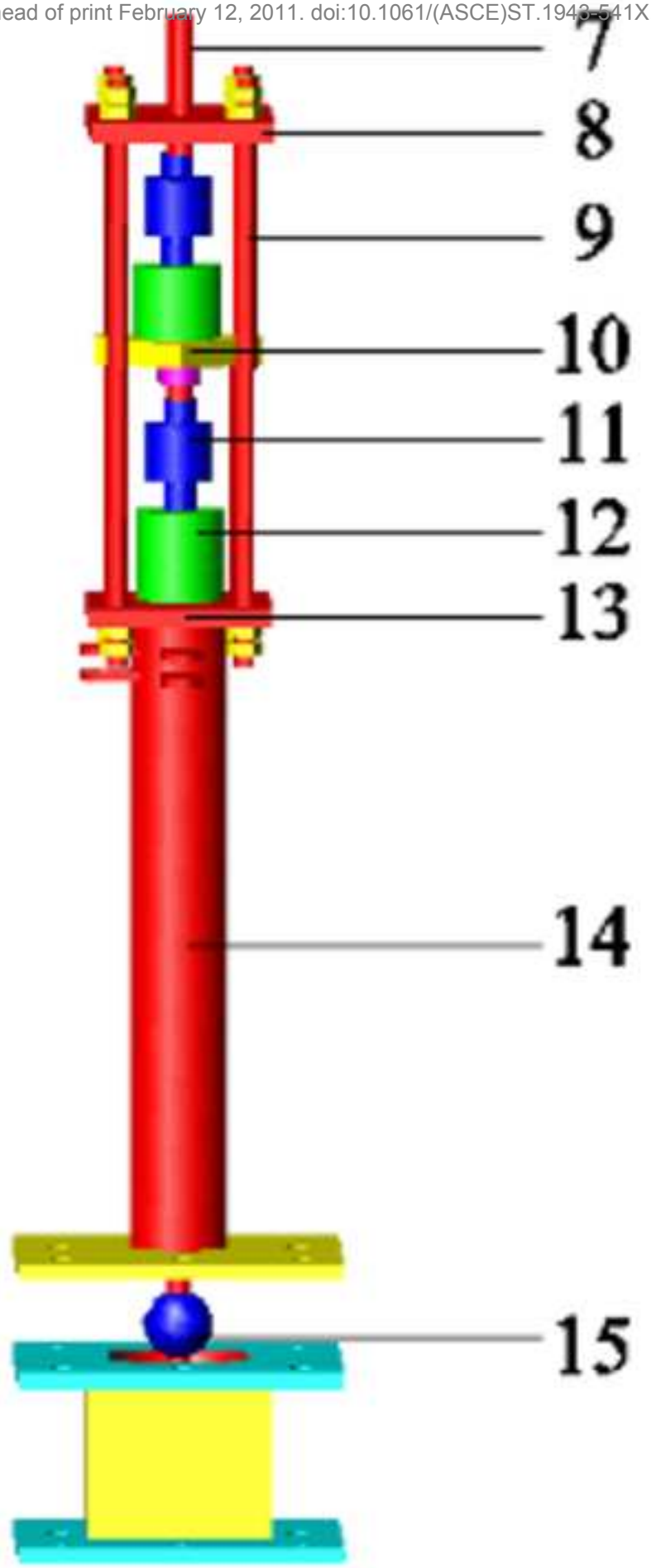

Journal of Structural Engineering. Submitted May 11, 2010; accepted February 10, 2011;
posted ahead of print February 12, 2011. doi:10.1061/(ASCE)ST.1943-541X.0000392

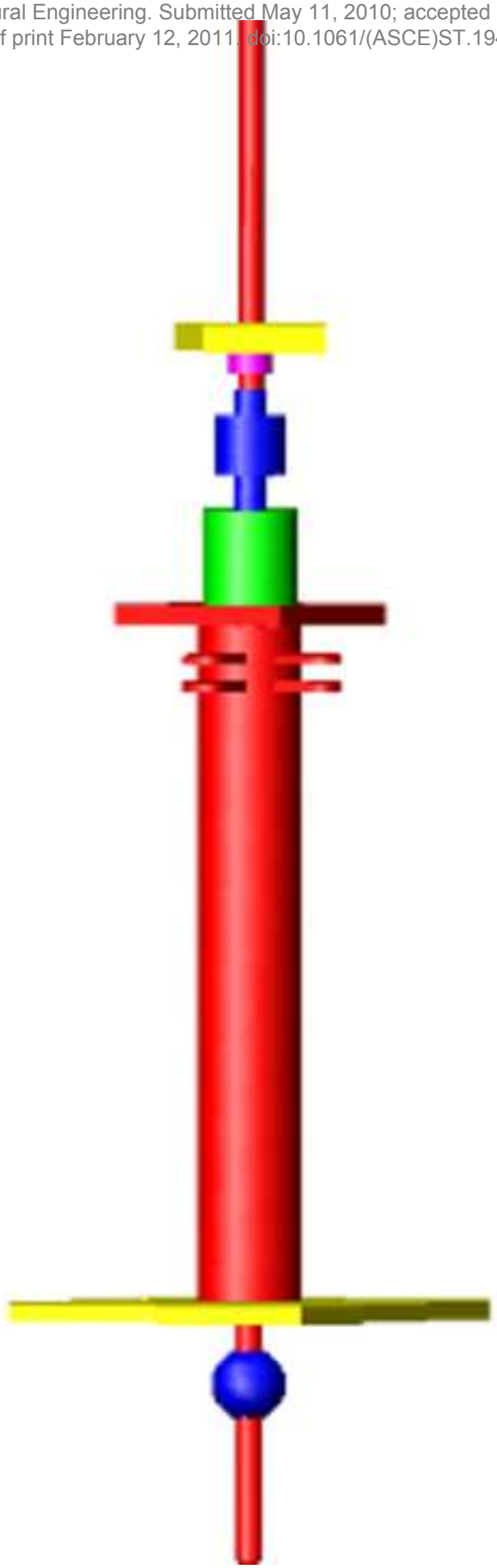

Journal of Structural Engineering. Submitted May 11, 2010; accepted February 10, 2011;
posted ahead of print February 12, 2011. doi:10.1061/(ASCE)ST.1943-541X.0000392

Journal of Structural Engineering. Submitted May 11, 2010; accepted February 10, 2011;
posted ahead of print February 12, 2011. doi:10.1061/(ASCE)ST.1943-541X.0000392

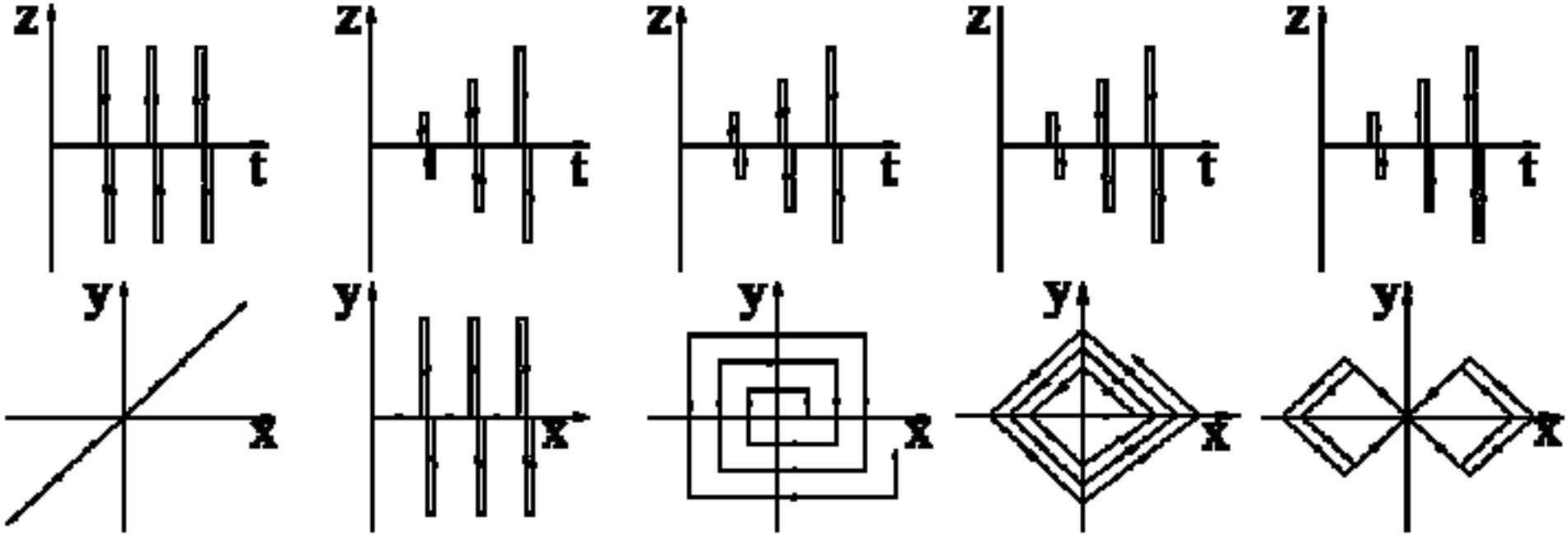

Journal of Structural Engineering. Submitted May 11, 2010; accepted February 10, 2011;
posted ahead of print February 12, 2011. doi:10.1061/(ASCE)ST.1943-541X.0000392

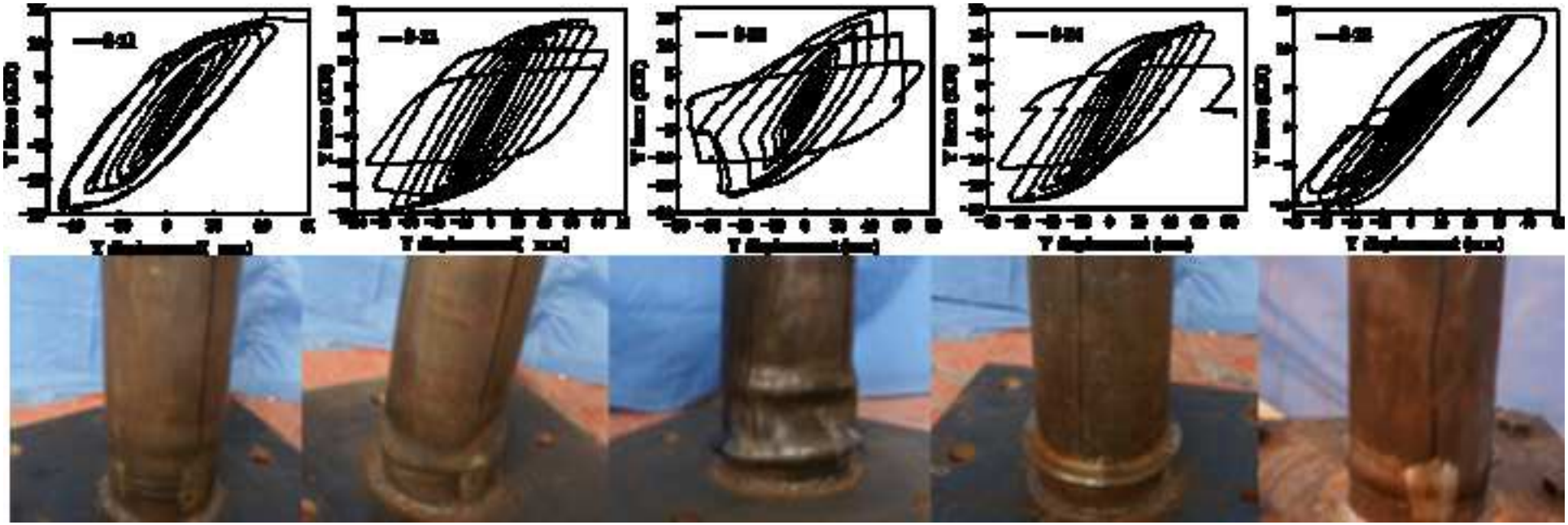

Journal of Structural Engineering. Submitted May 11, 2010; accepted February 10, 2011;
posted ahead of print February 12, 2011. doi:10.1061/(ASCE)ST.1943-541X.0000392

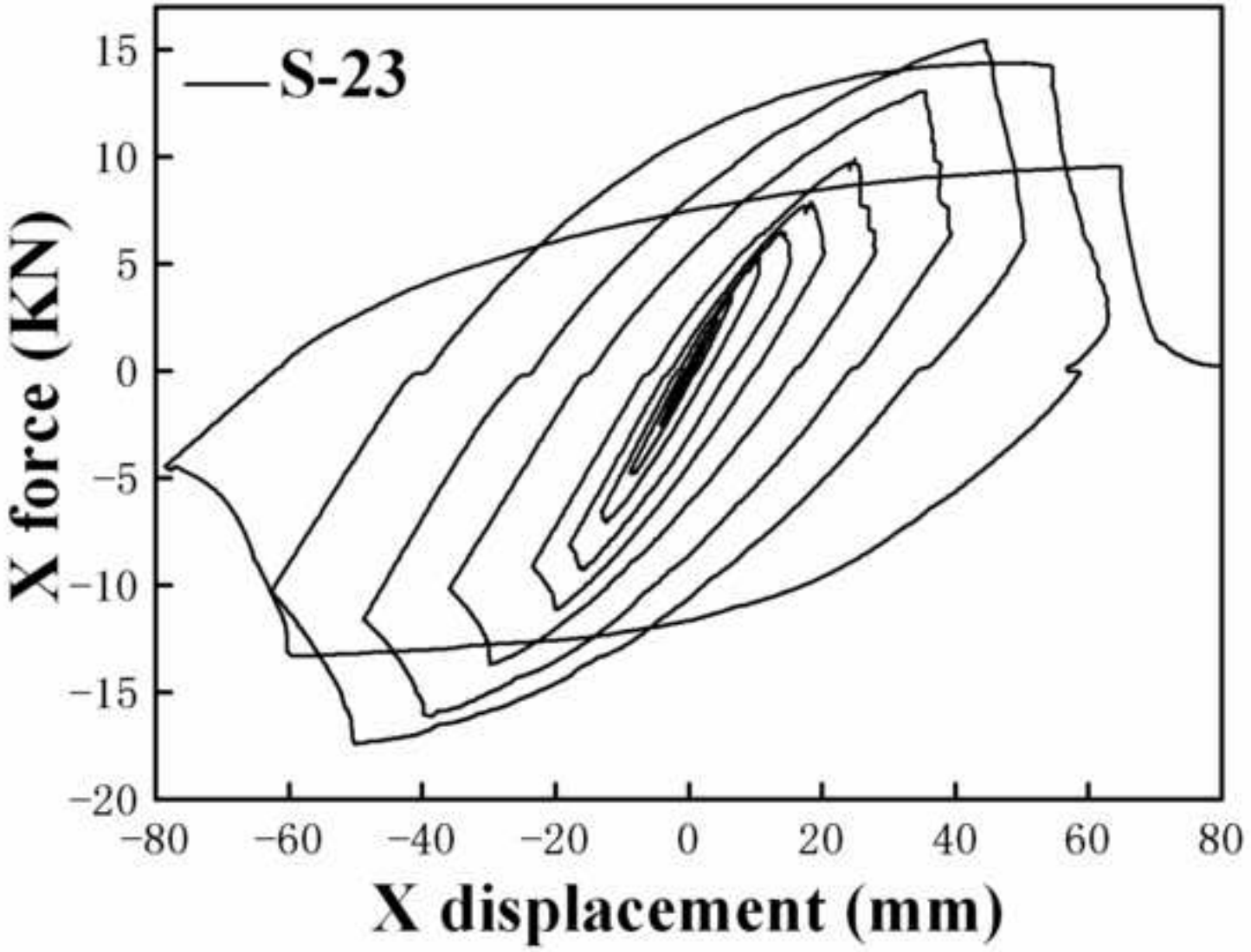

Journal of Structural Engineering. Submitted May 11, 2010; accepted February 10, 2011;
posted ahead of print February 12, 2011. doi:10.1061/(ASCE)ST.1943-541X.0000392

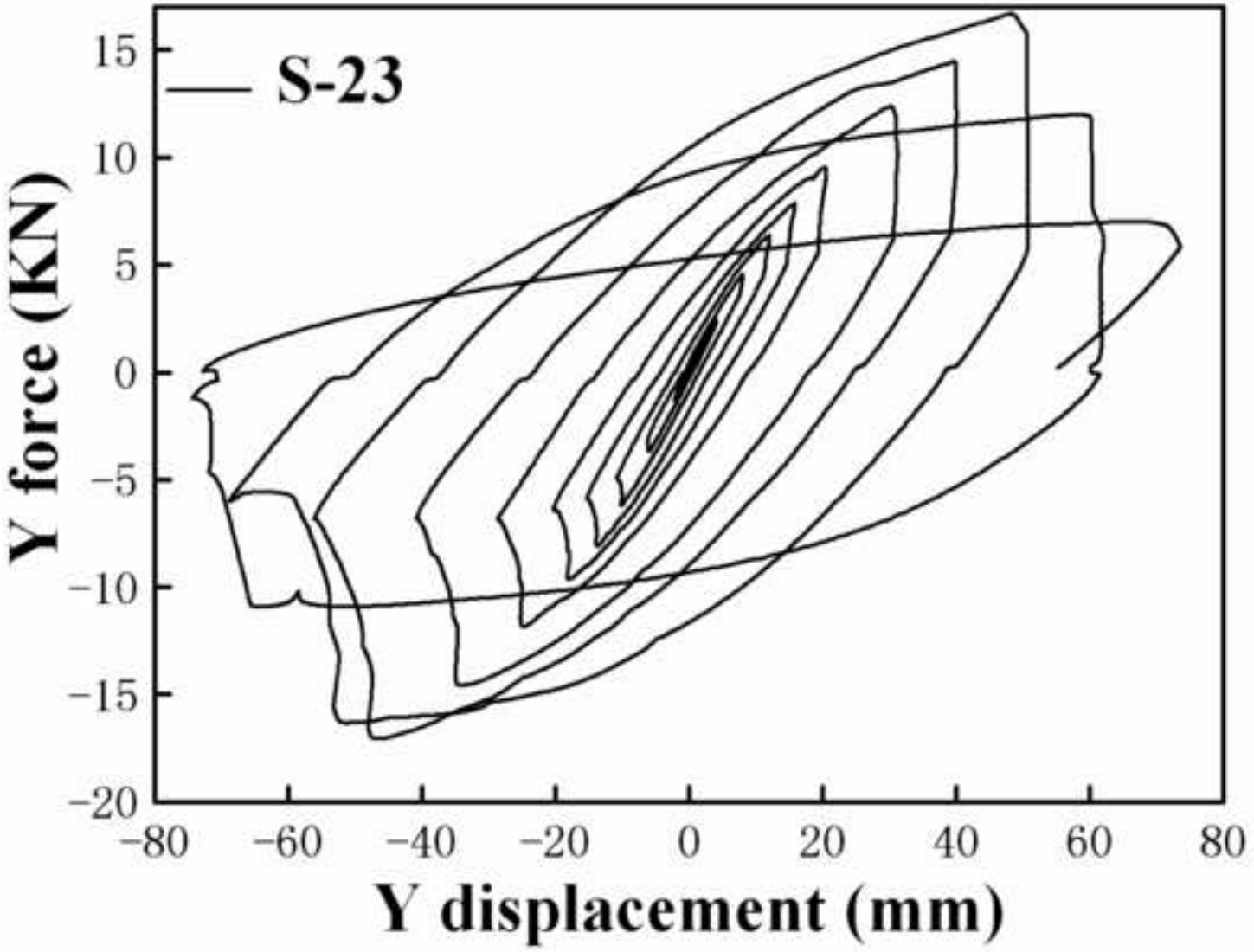

Journal of Structural Engineering. Submitted May 11, 2010; accepted February 10, 2011;
posted ahead of print February 12, 2011. doi:10.1061/(ASCE)ST.1943-541X.0000392

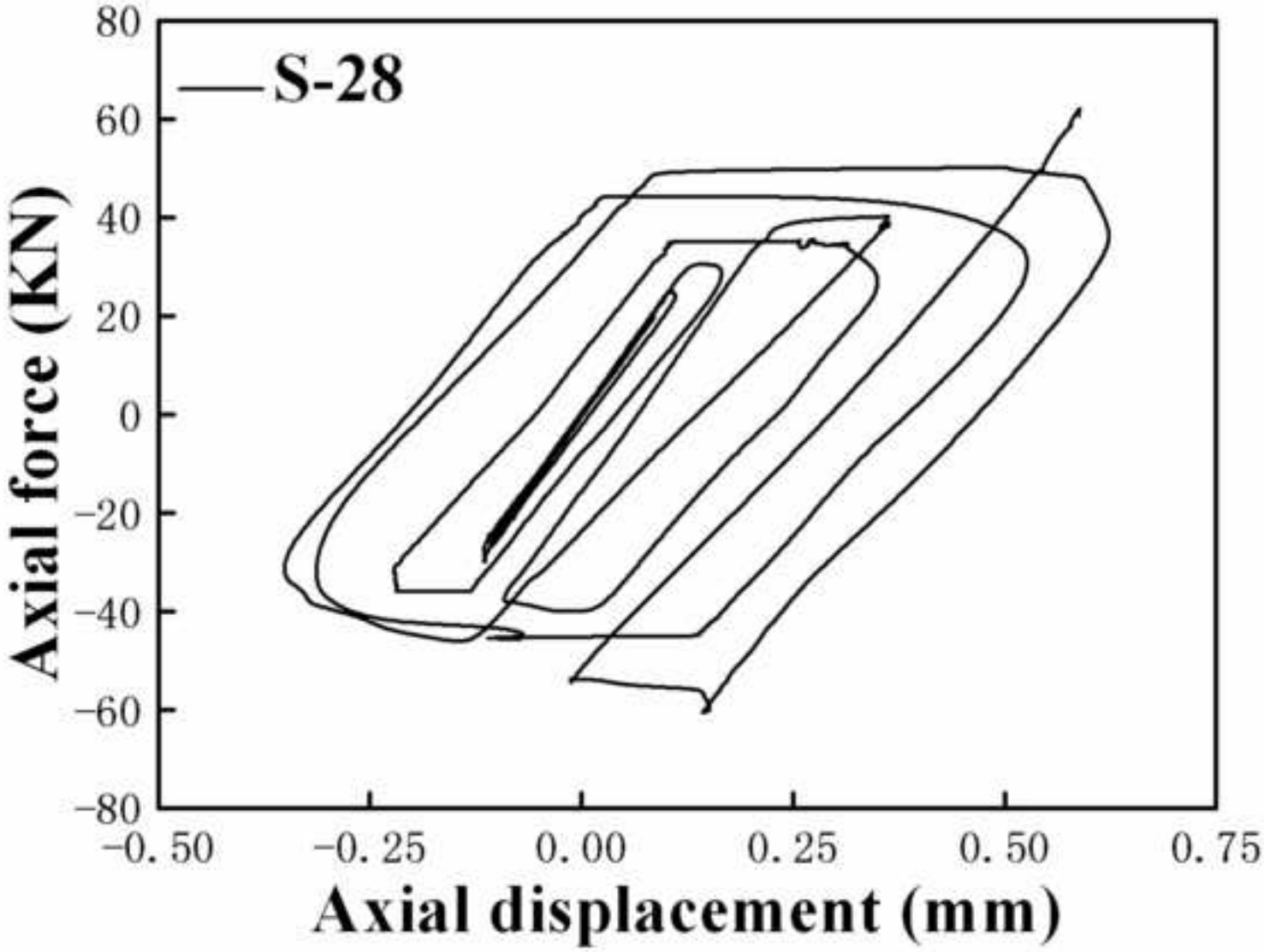

Journal of Structural Engineering. Submitted May 11, 2010; accepted February 10, 2011;
posted ahead of print February 12, 2011. doi:10.1061/(ASCE)ST.1943-541X.0000392

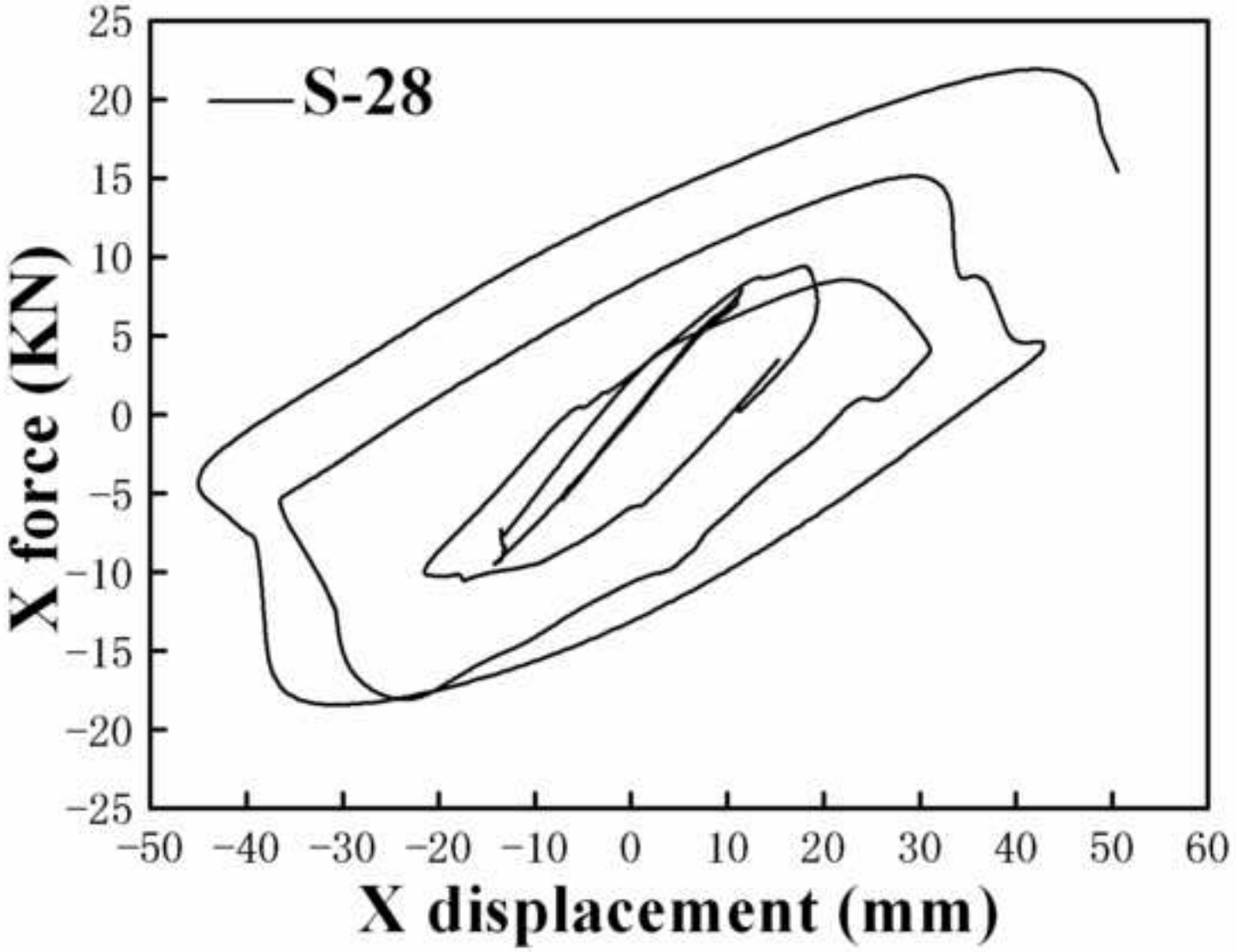

Journal of Structural Engineering. Submitted May 11, 2010; accepted February 10, 2011;
posted ahead of print February 12, 2011. doi:10.1061/(ASCE)ST.1943-541X.0000392

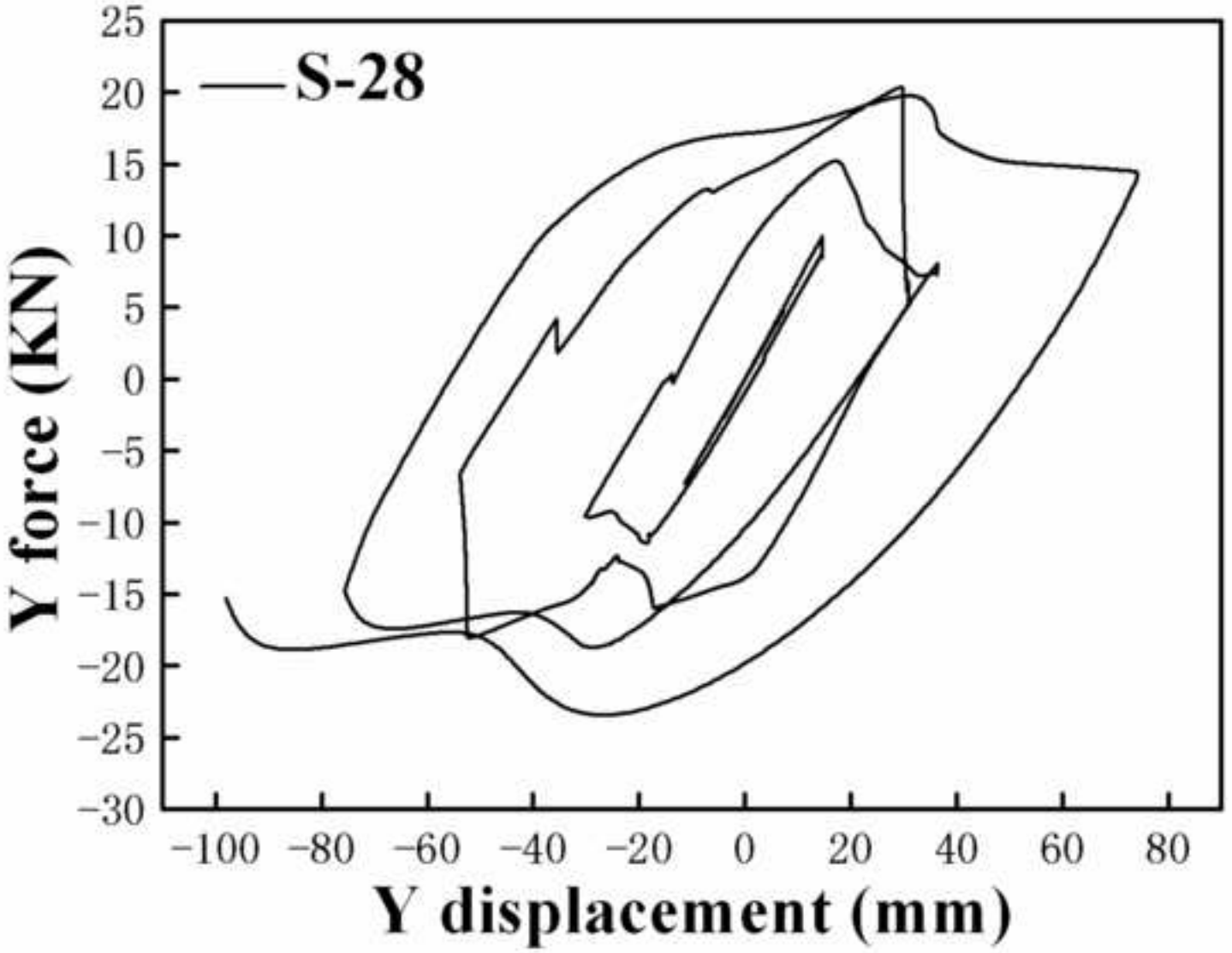

Journal of Structural Engineering. Submitted May 11, 2010; accepted February 10, 2011;
posted ahead of print February 12, 2011. doi:10.1061/(ASCE)ST.1943-541X.0000392

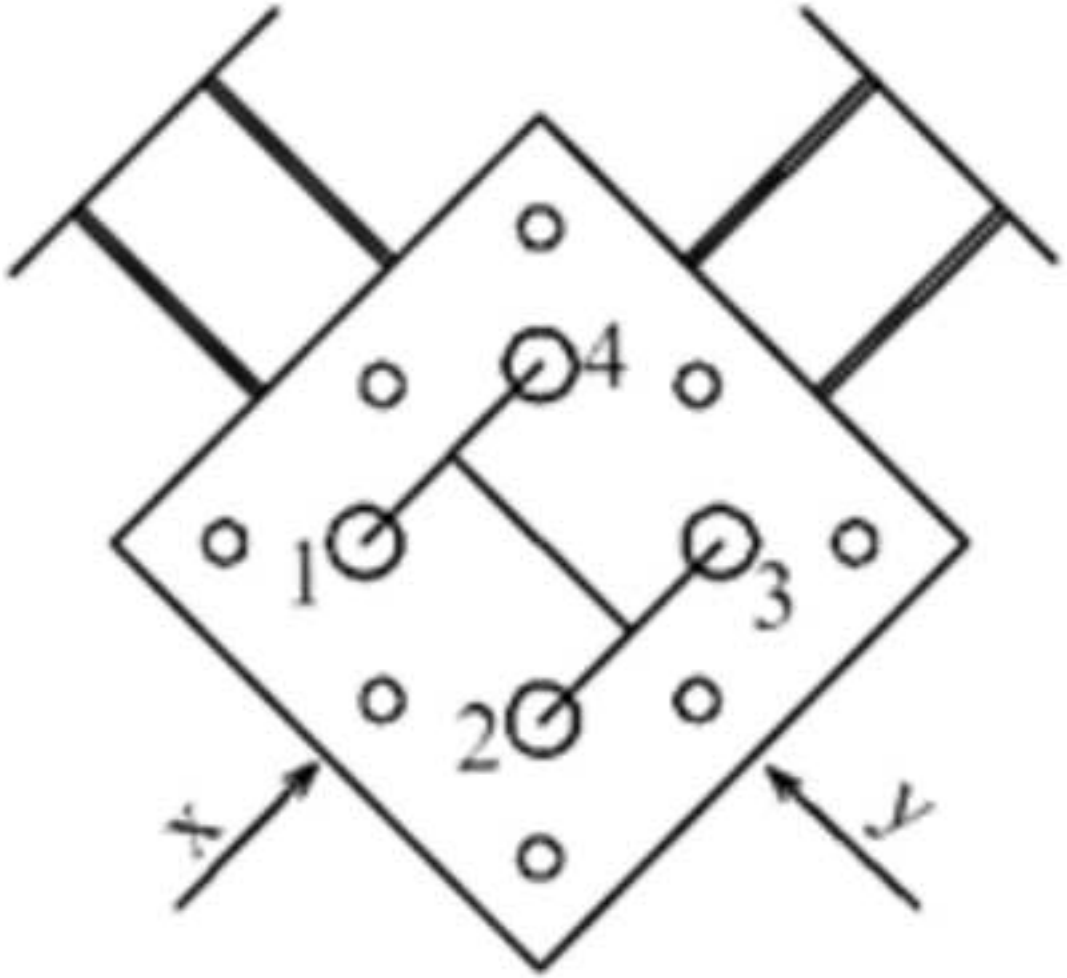

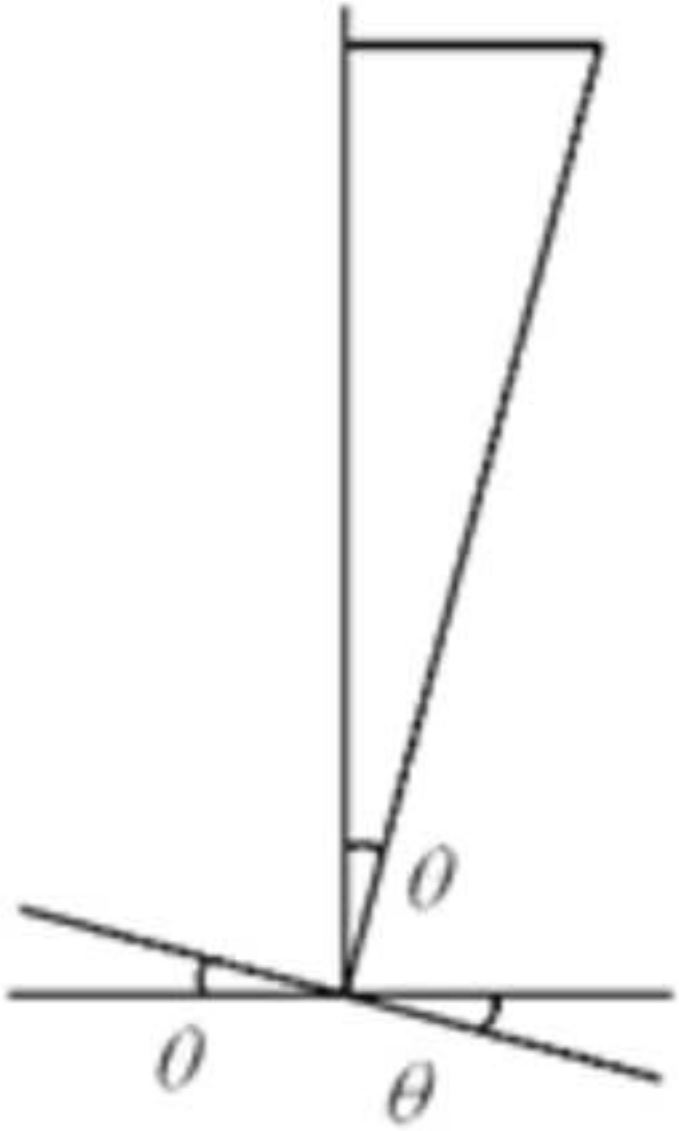

Journal of Structural Engineering. Submitted May 11, 2010; accepted February 10, 2011;
posted ahead of print February 12, 2011. doi:10.1061/(ASCE)ST.1943-541X.0000392

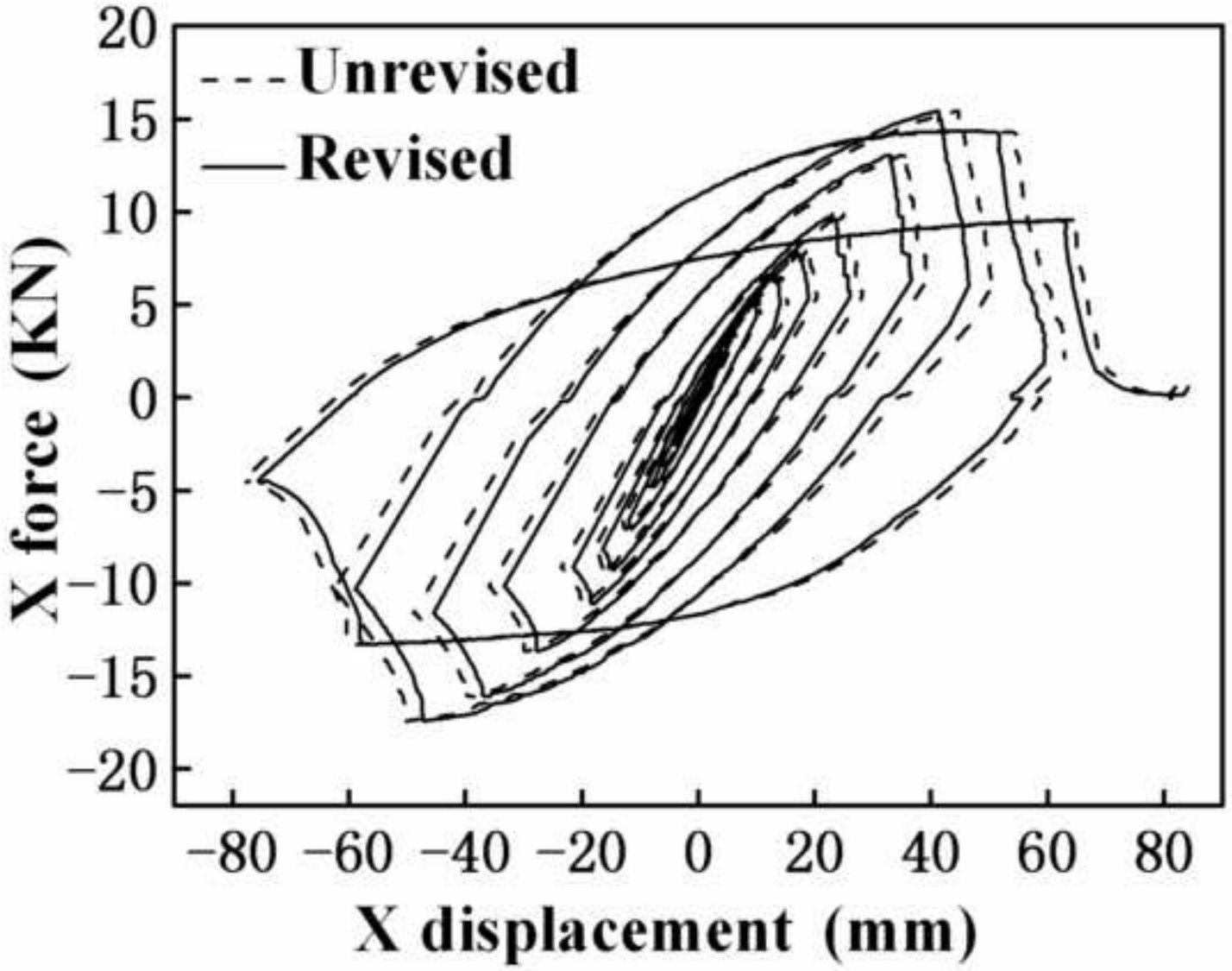

Journal of Structural Engineering. Submitted May 11, 2010; accepted February 10, 2011;
posted ahead of print February 12, 2011. doi:10.1061/(ASCE)ST.1943-541X.0000392

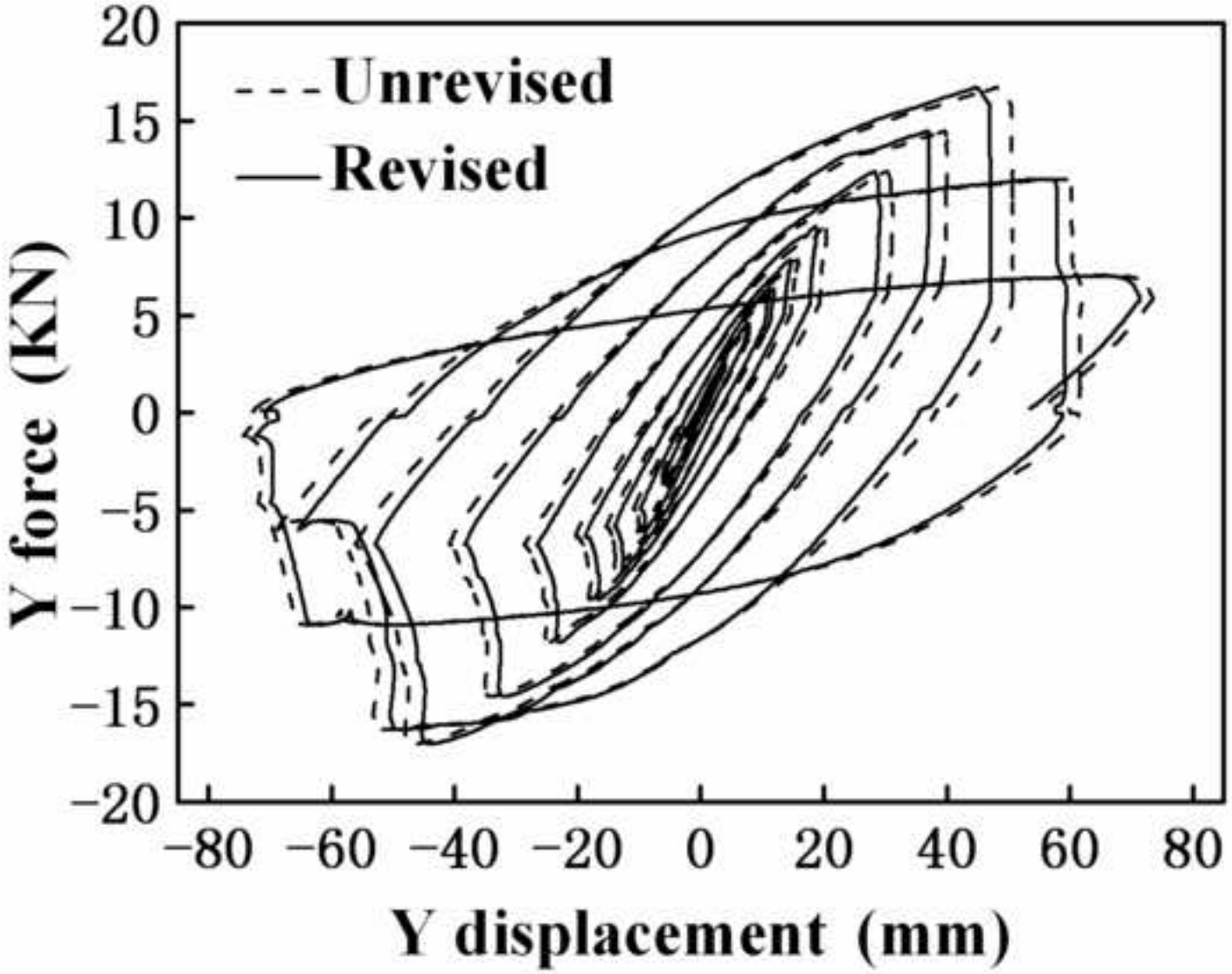

Journal of Structural Engineering. Submitted May 11, 2010; accepted February 10, 2011;
posted ahead of print February 12, 2011. doi:10.1061/(ASCE)ST.1943-541X.0000392

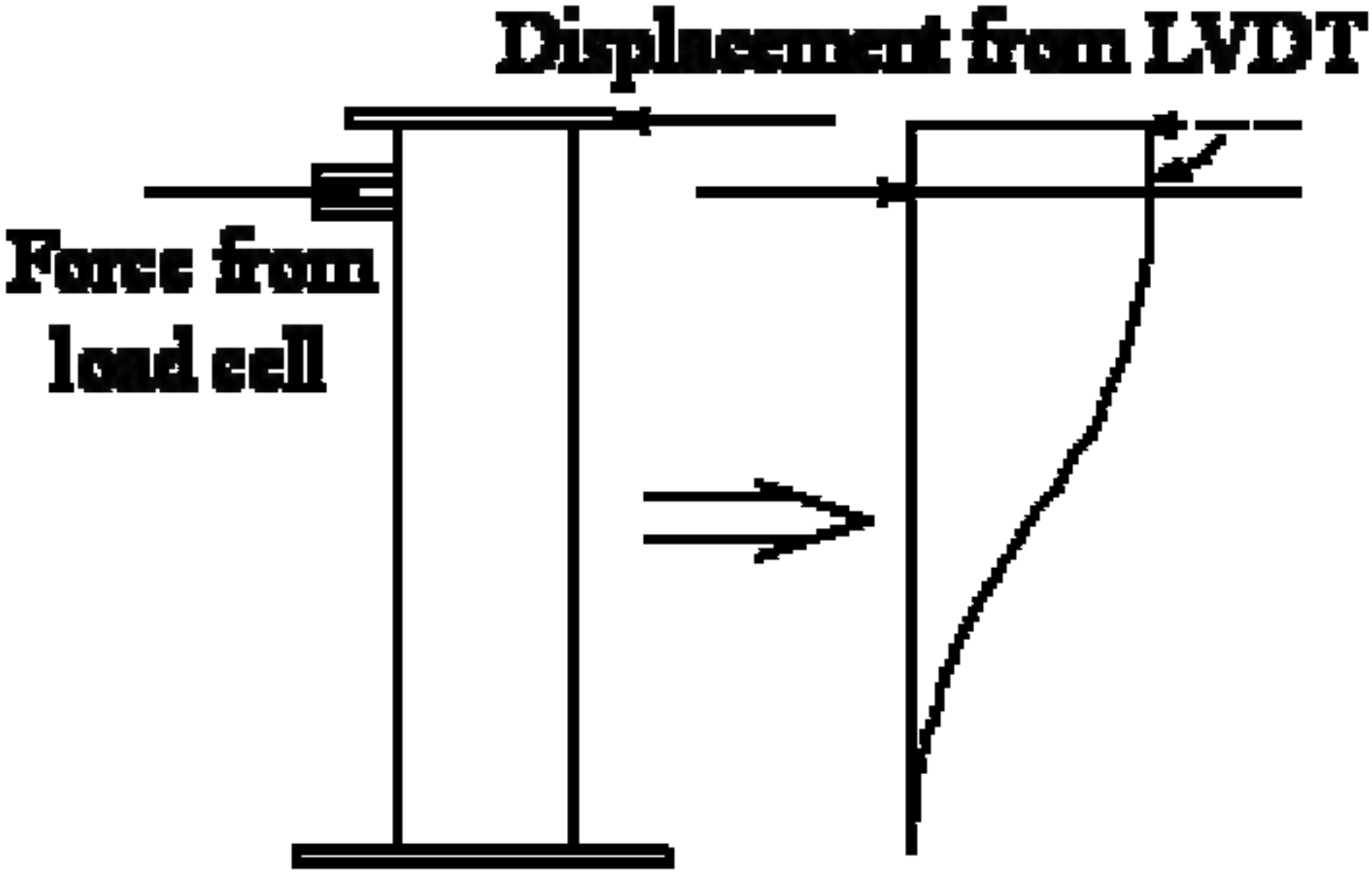

Journal of Structural Engineering. Submitted May 11, 2010; accepted February 10, 2011;
posted ahead of print February 12, 2011. doi:10.1061/(ASCE)ST.1943-541X.0000392

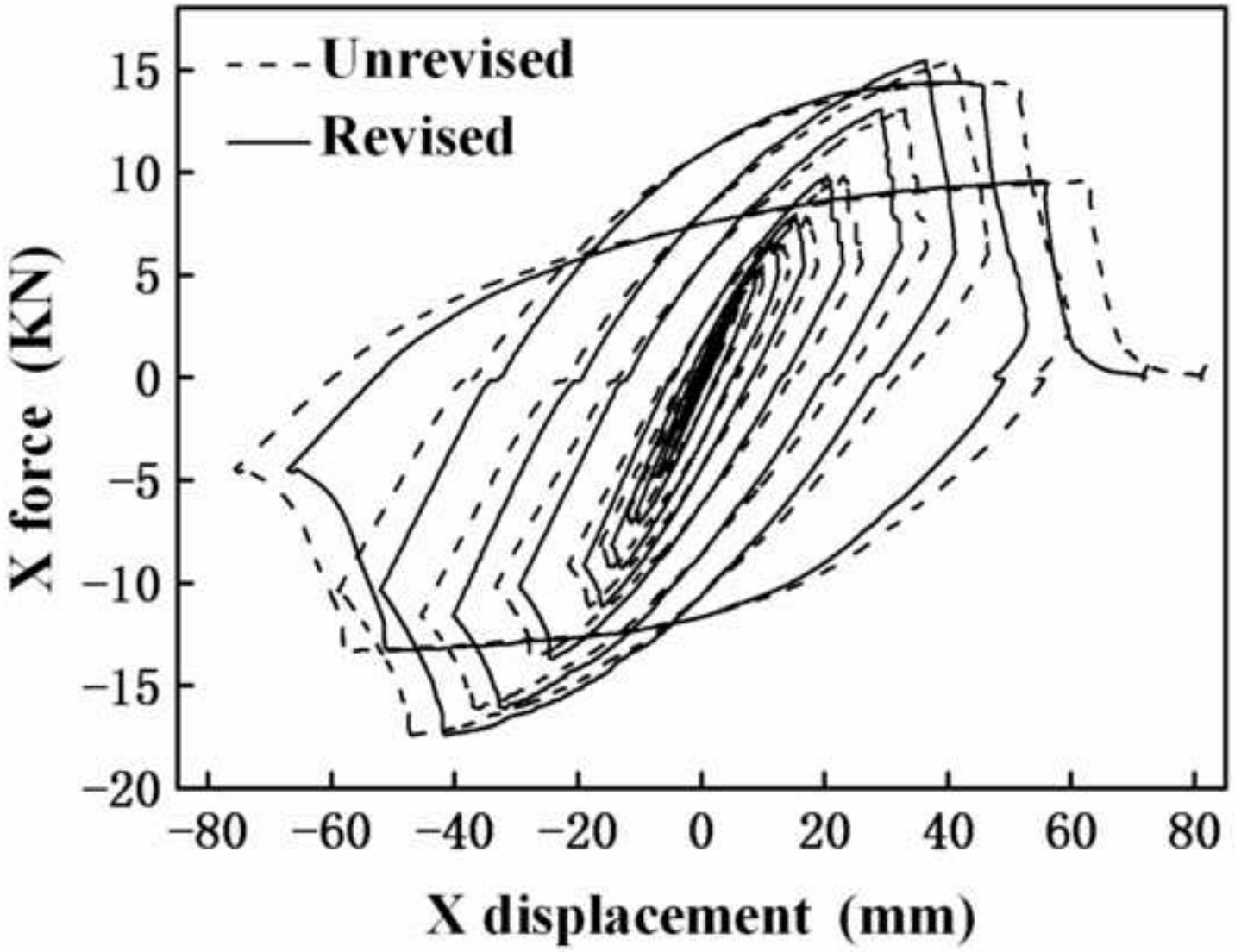

Journal of Structural Engineering. Submitted May 11, 2010; accepted February 10, 2011;
posted ahead of print February 12, 2011. doi:10.1061/(ASCE)ST.1943-541X.0000392

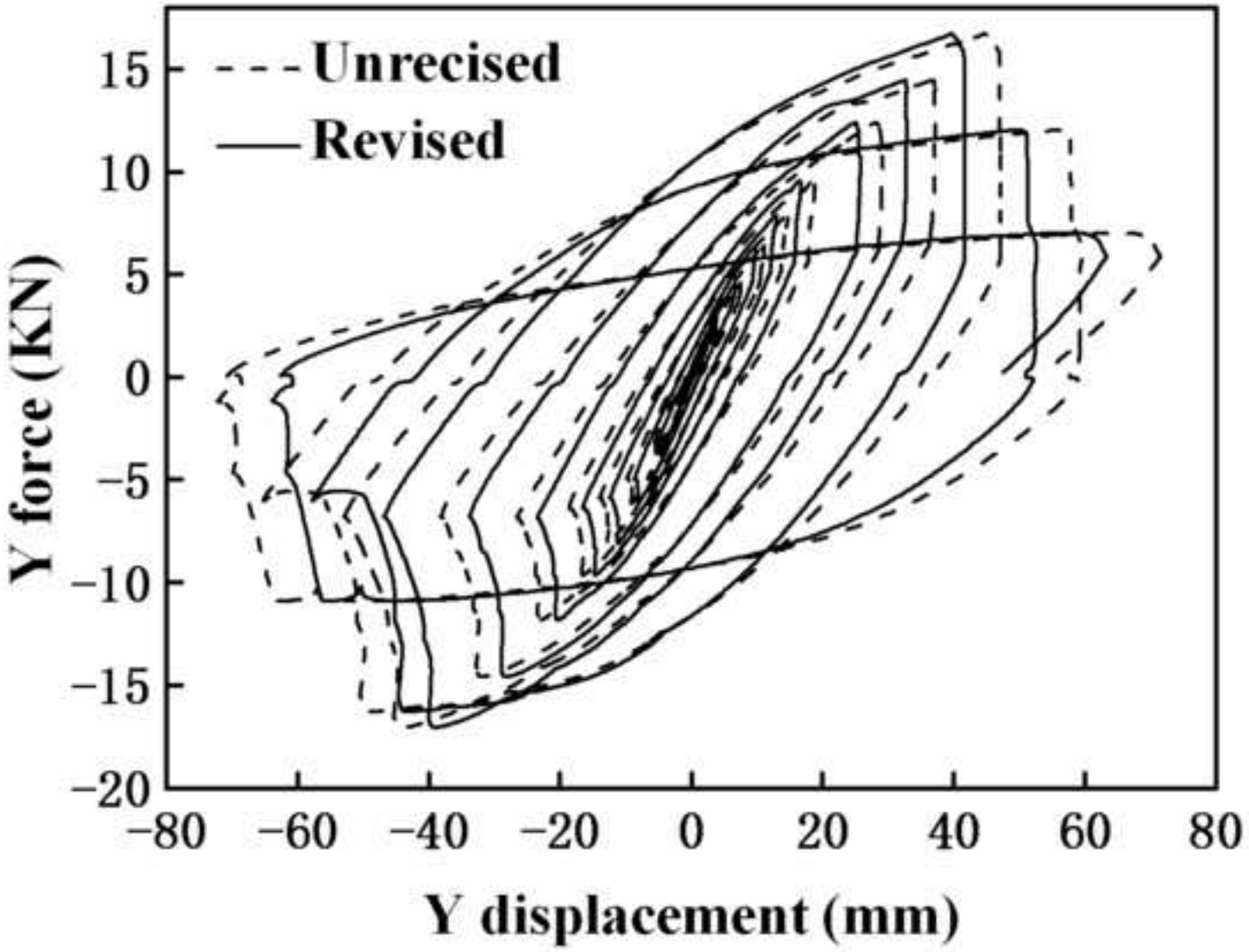

Journal of Structural Engineering. Submitted May 11, 2010; accepted February 10, 2011;
posted ahead of print February 12, 2011. doi:10.1061/(ASCE)ST.1943-541X.0000392

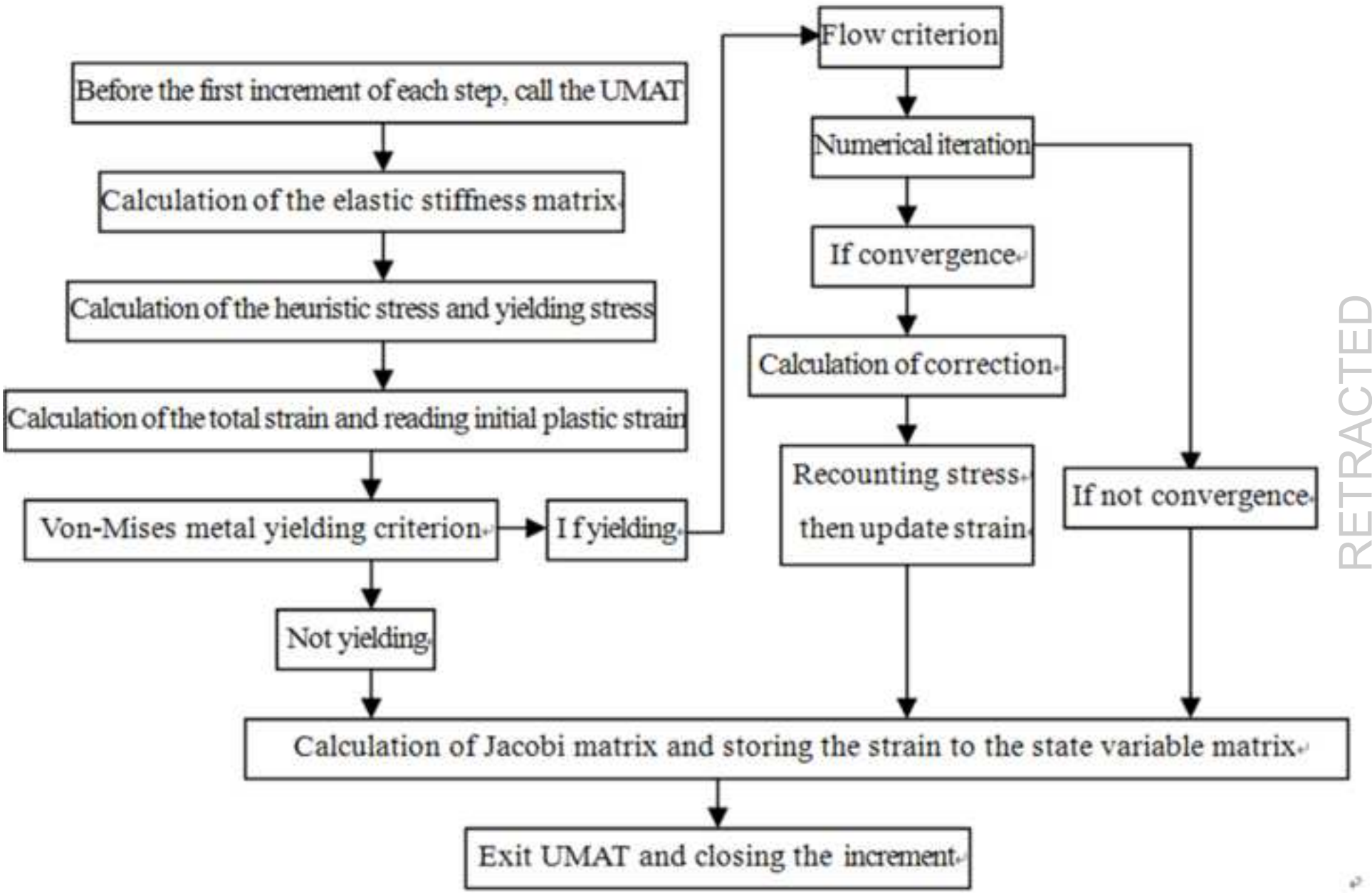

Journal of Structural Engineering. Submitted May 11, 2010; accepted February 10, 2011;
posted ahead of print February 12, 2011. doi:10.1061/(ASCE)ST.1943-541X.0000392

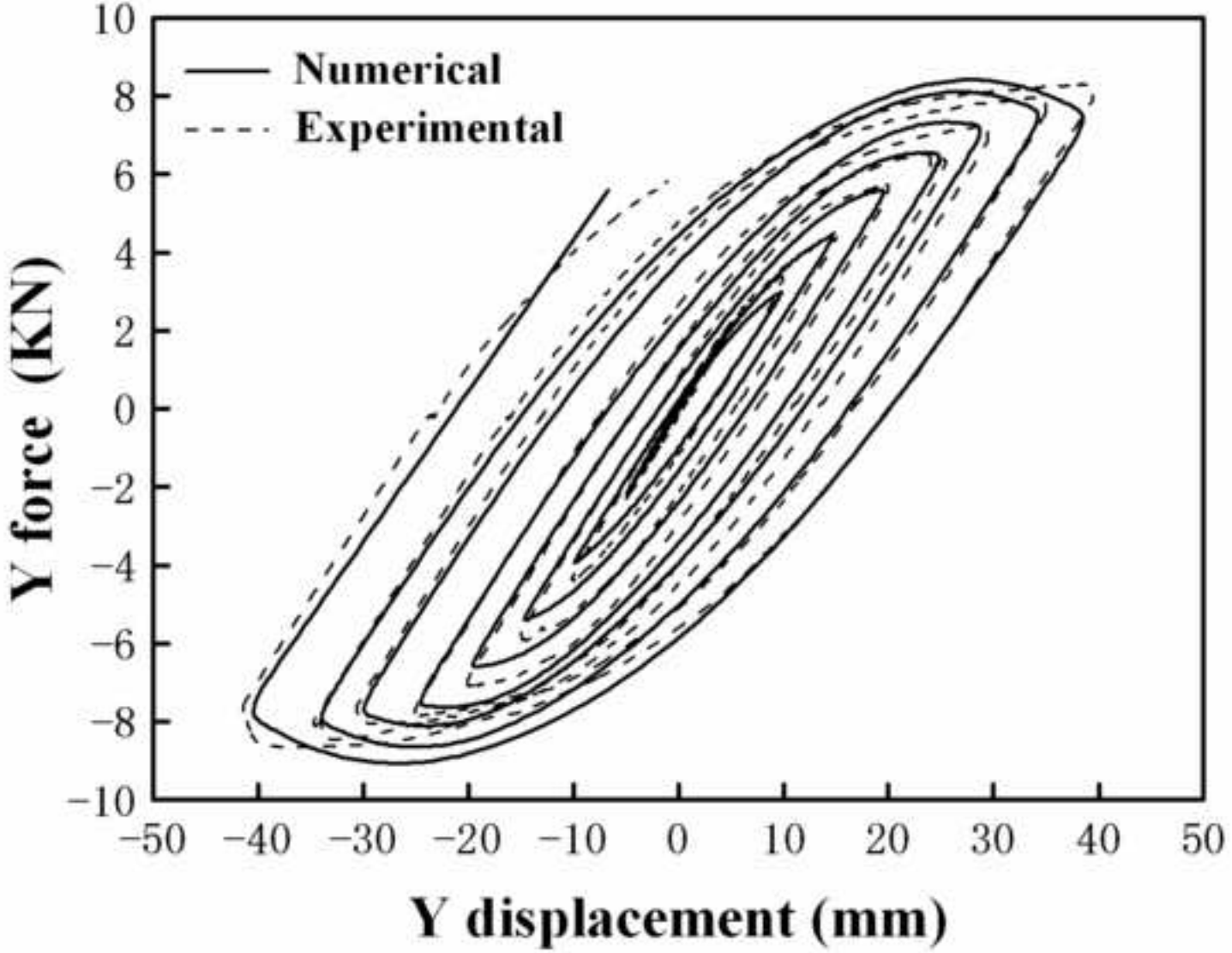

Journal of Structural Engineering. Submitted May 11, 2010; accepted February 10, 2011;
posted ahead of print February 12, 2011. doi:10.1061/(ASCE)ST.1943-541X.0000392

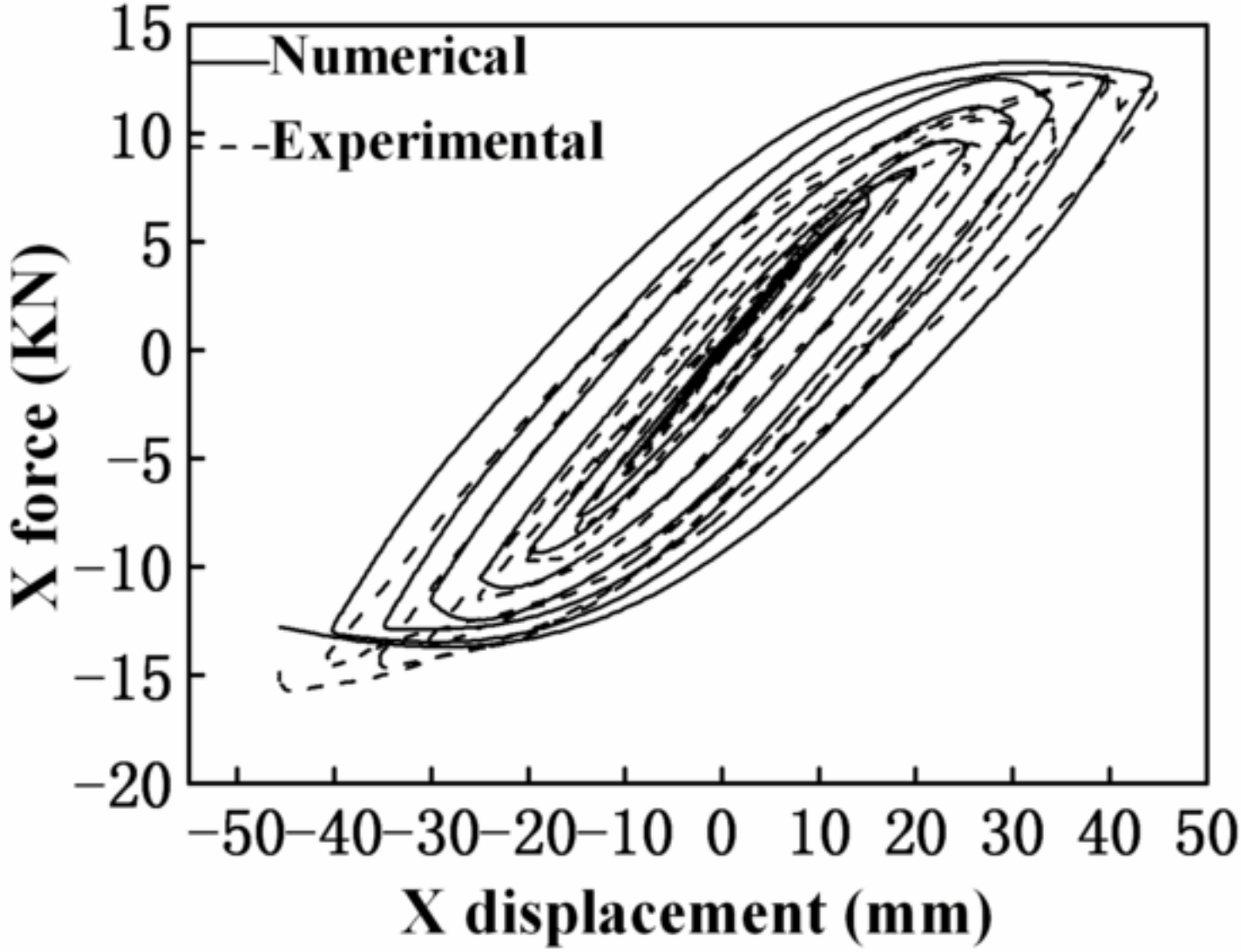

Journal of Structural Engineering. Submitted May 11, 2010; accepted February 10, 2011;
posted ahead of print February 12, 2011. doi:10.1061/(ASCE)ST.1943-541X.0000392

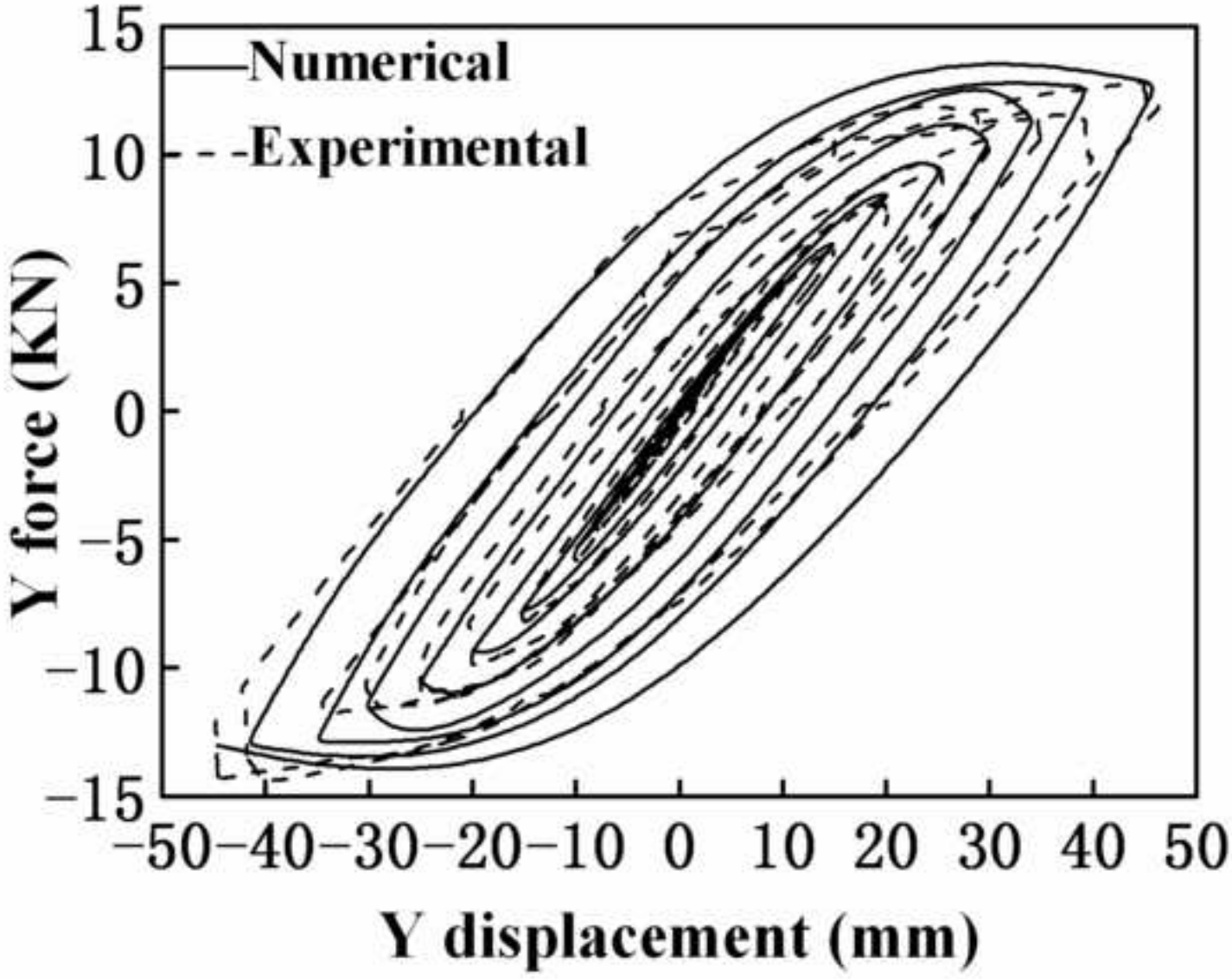

Journal of Structural Engineering. Submitted May 11, 2010; accepted February 10, 2011;
posted ahead of print February 12, 2011. doi:10.1061/(ASCE)ST.1943-541X.0000392

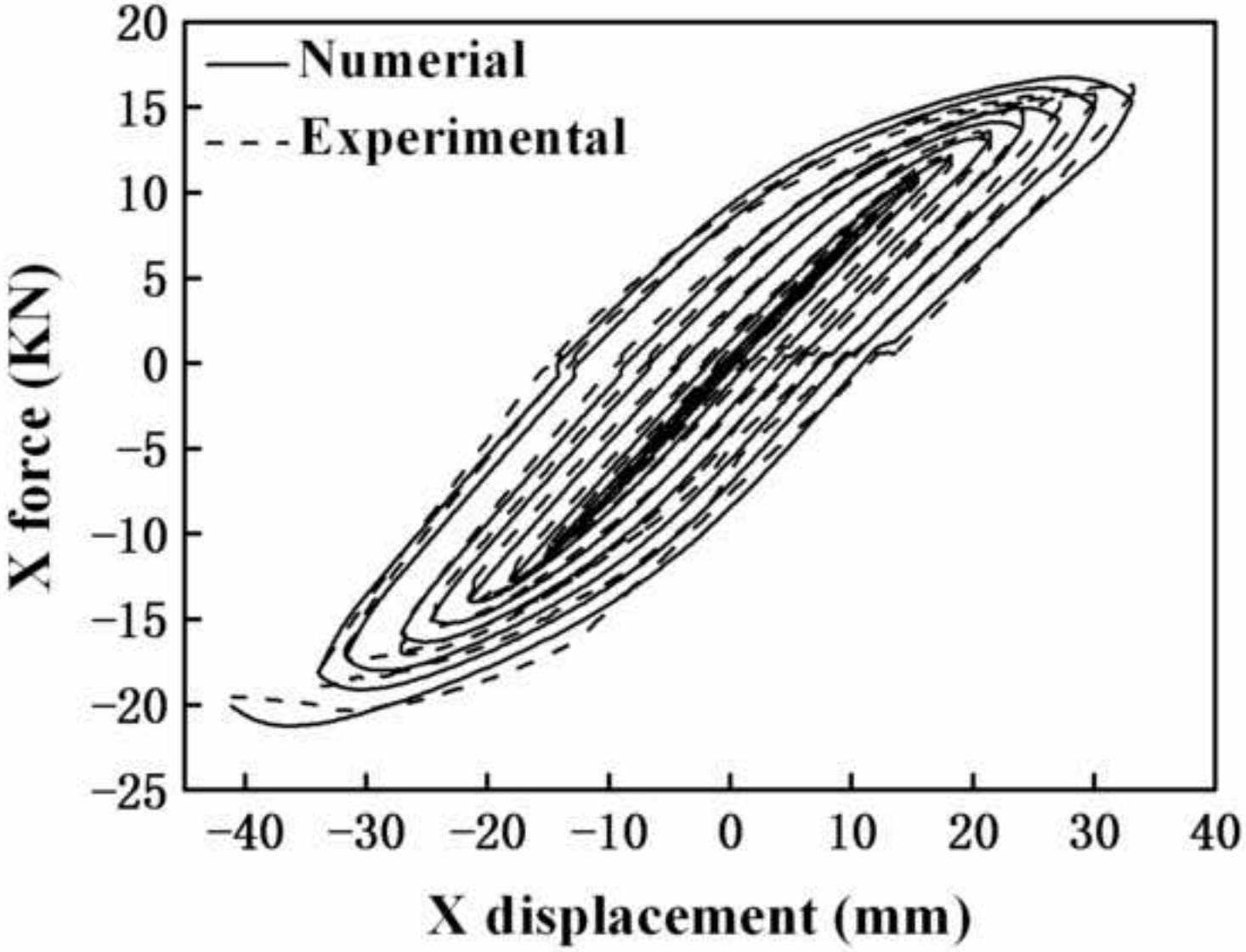

Journal of Structural Engineering. Submitted May 11, 2010; accepted February 10, 2011;
posted ahead of print February 12, 2011. doi:10.1061/(ASCE)ST.1943-541X.0000392

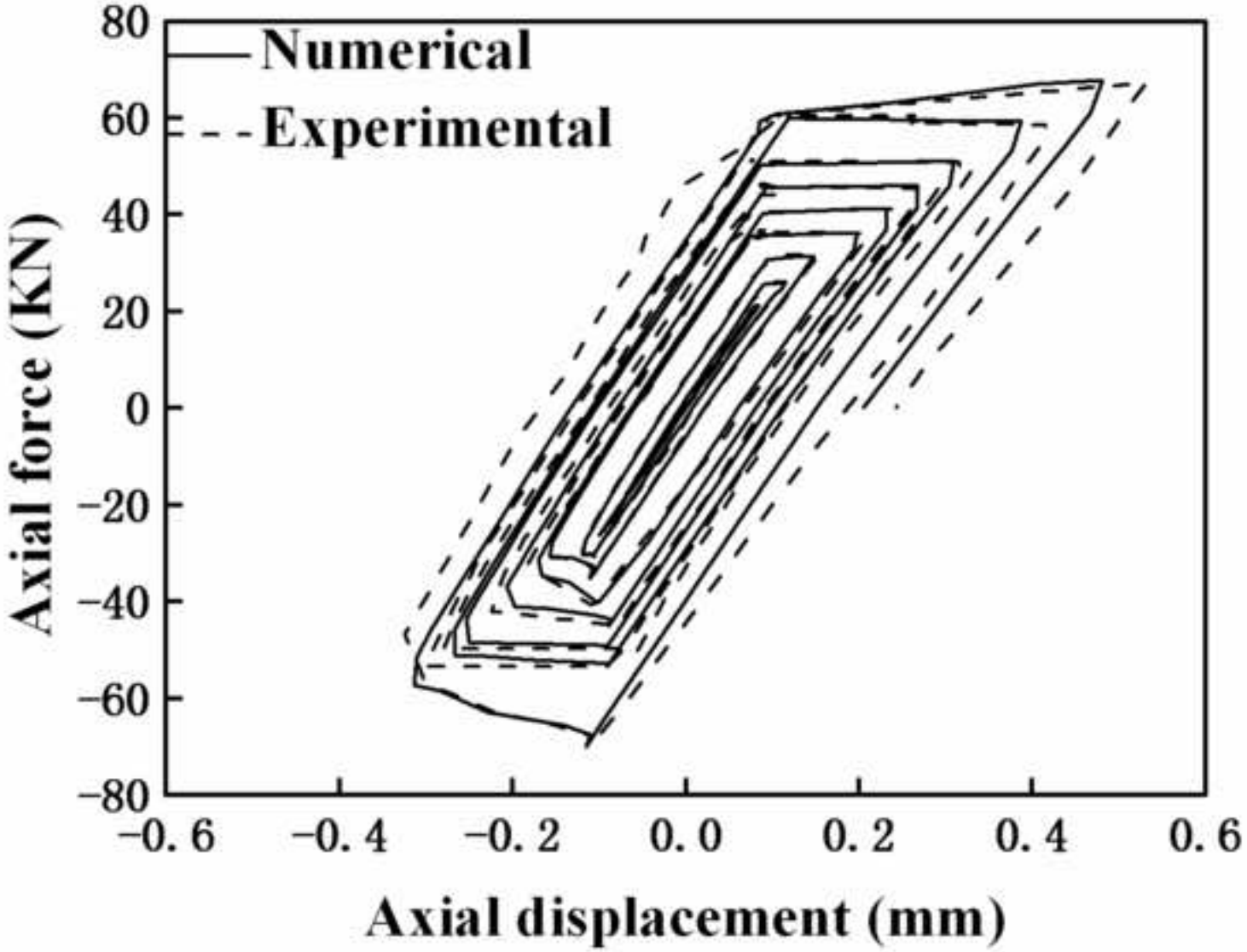

Journal of Structural Engineering. Submitted May 11, 2010; accepted February 10, 2011;
posted ahead of print February 12, 2011. doi:10.1061/(ASCE)ST.1943-541X.0000392

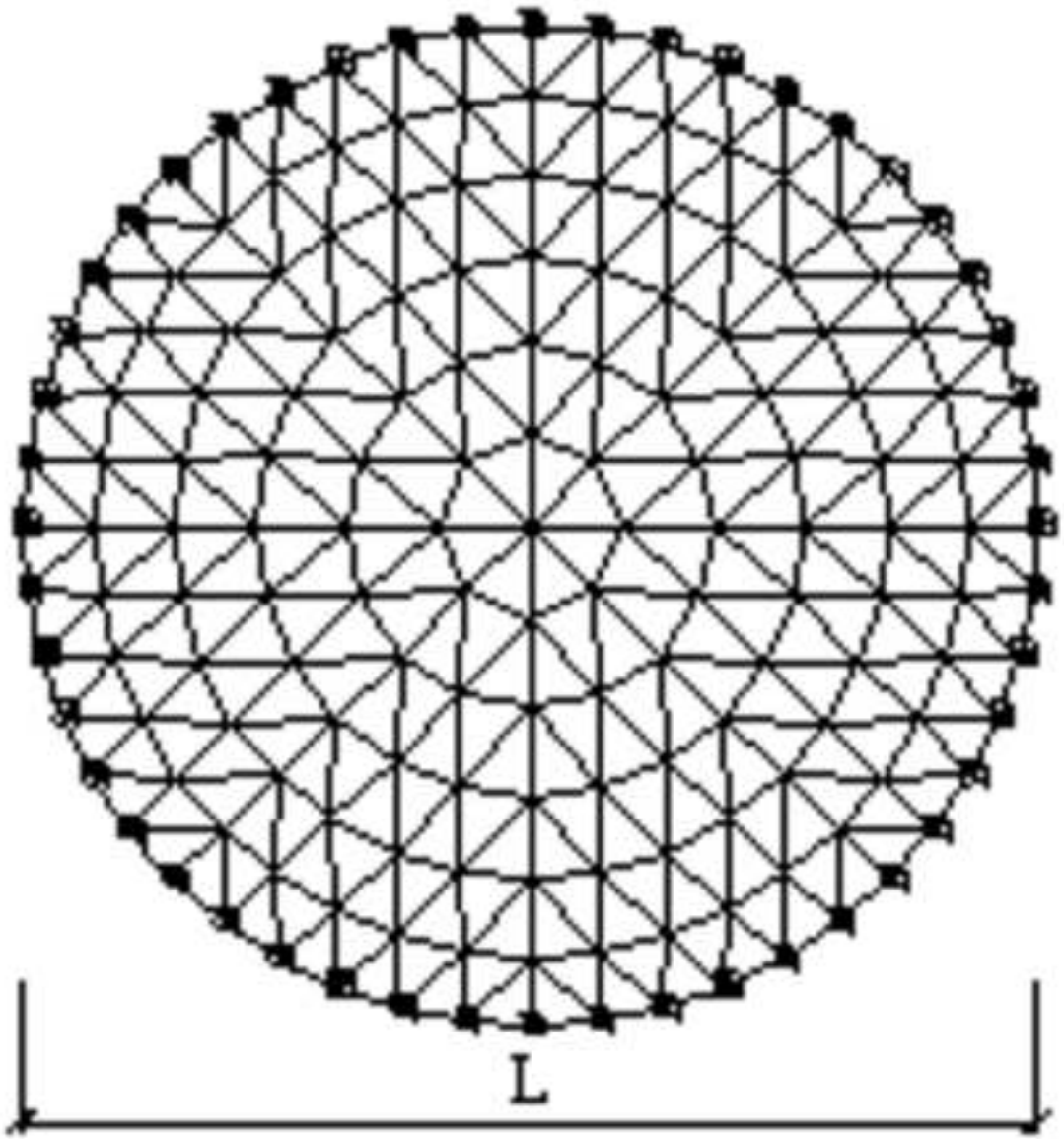

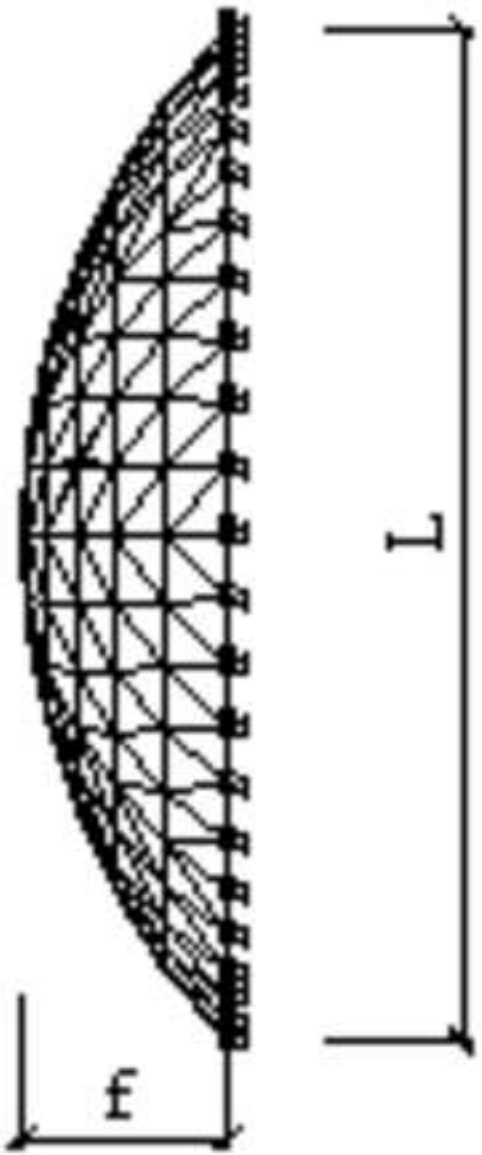

Journal of Structural Engineering. Submitted May 11, 2010; accepted February 10, 2011;
posted ahead of print February 12, 2011. doi:10.1061/(ASCE)ST.1943-541X.0000392

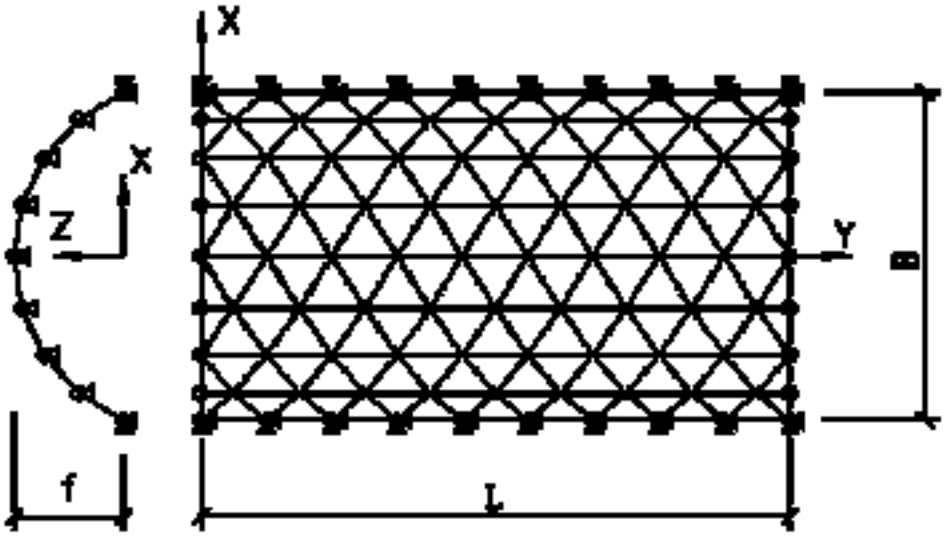

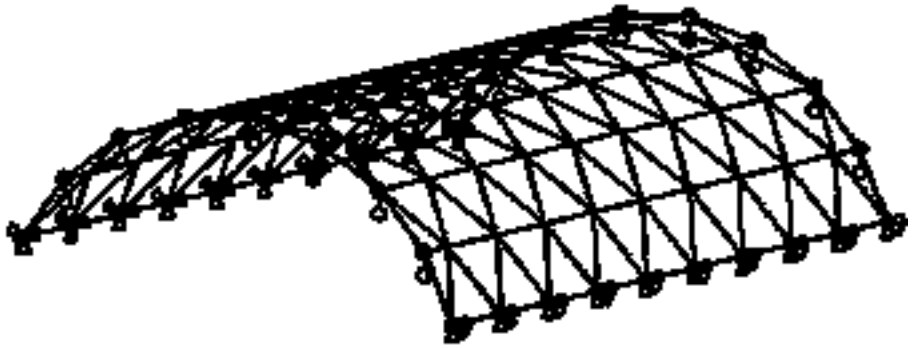

RETRACTED

Journal of Structural Engineering. Submitted May 11, 2010; accepted February 10, 2011;
posted ahead of print February 12, 2011. doi:10.1061/(ASCE)ST.1943-541X.0000392

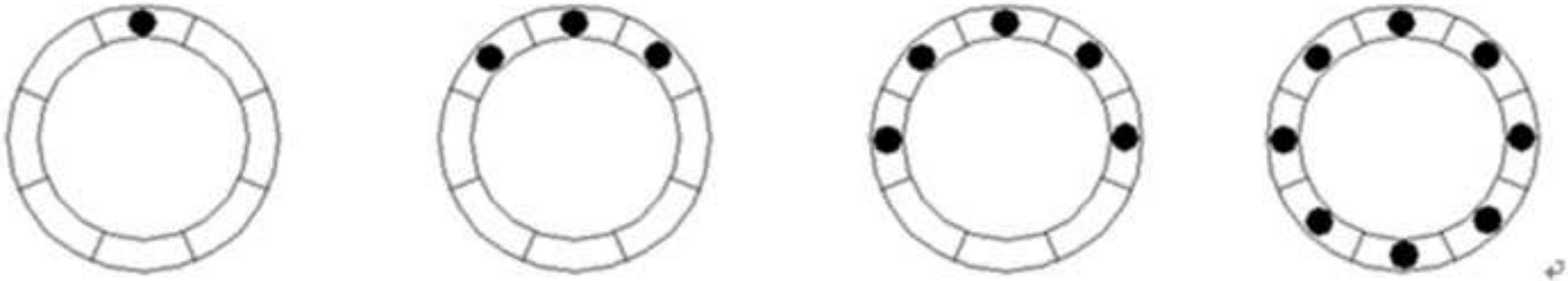

Journal of Structural Engineering. Submitted May 11, 2010; accepted February 10, 2011;
posted ahead of print February 12, 2011. doi:10.1061/(ASCE)ST.1943-541X.0000392

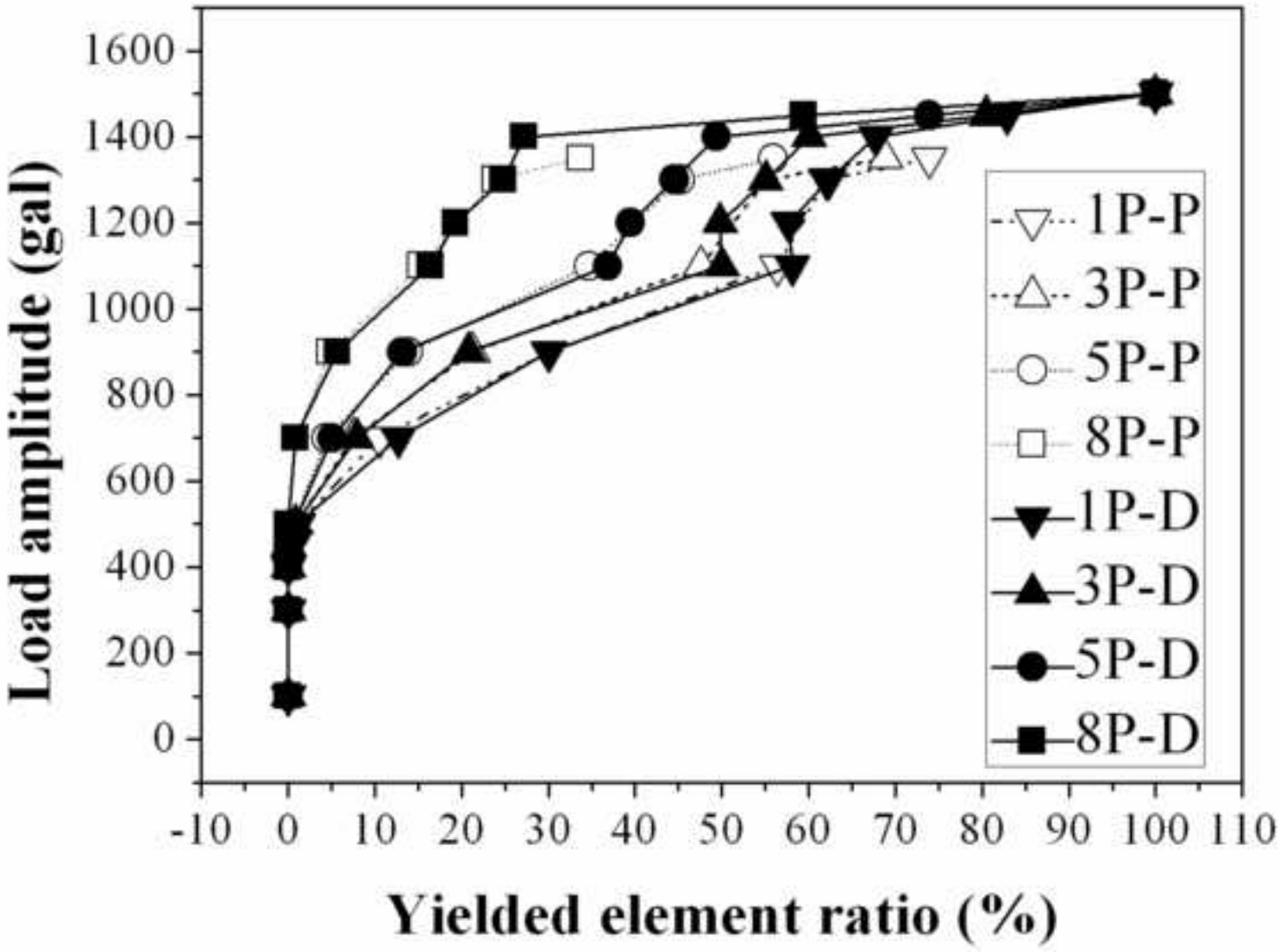

Journal of Structural Engineering. Submitted May 11, 2010; accepted February 10, 2011;
posted ahead of print February 12, 2011. doi:10.1061/(ASCE)ST.1943-541X.0000392

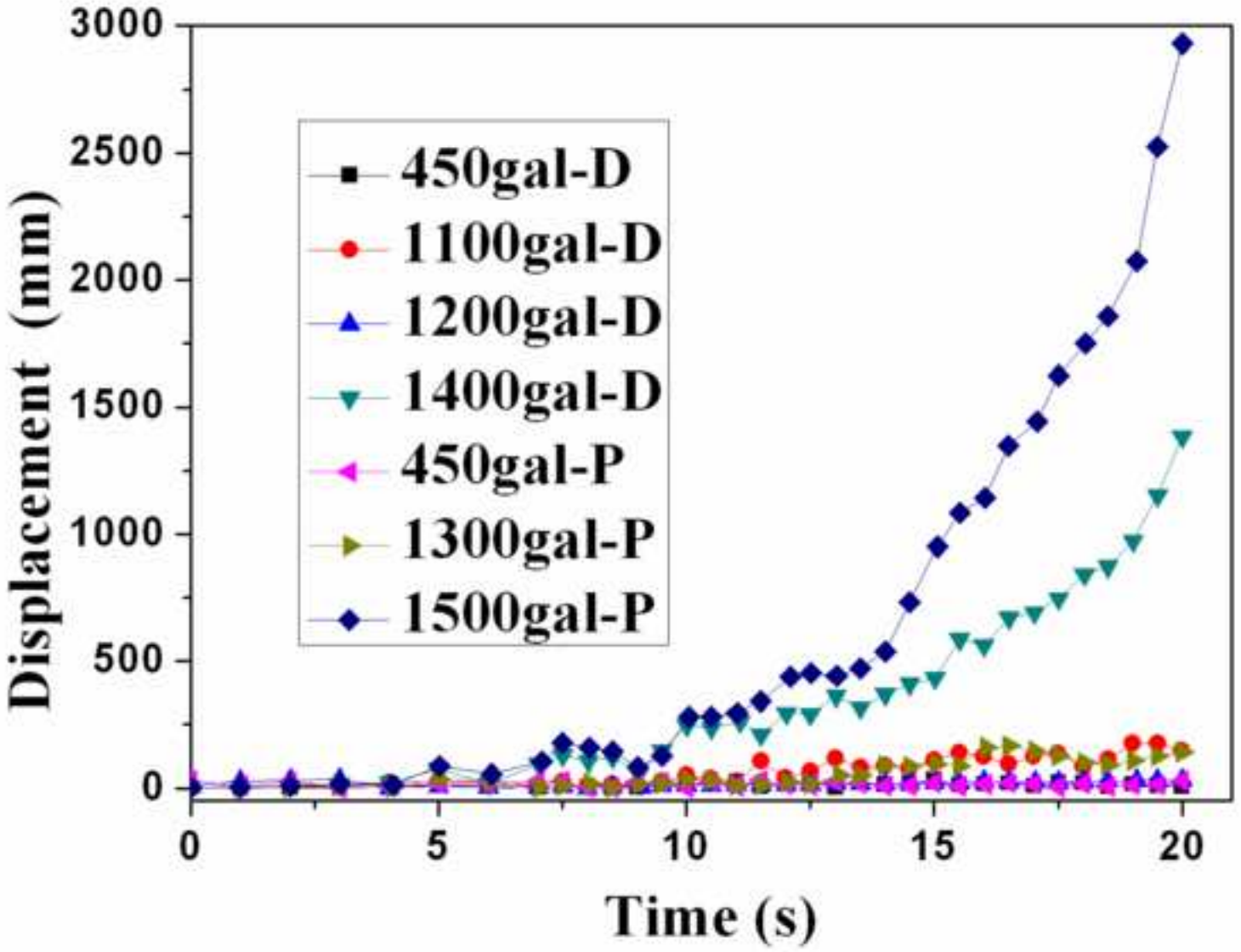

Journal of Structural Engineering. Submitted May 11, 2010; accepted February 10, 2011;
posted ahead of print February 12, 2011. doi:10.1061/(ASCE)ST.1943-541X.0000392

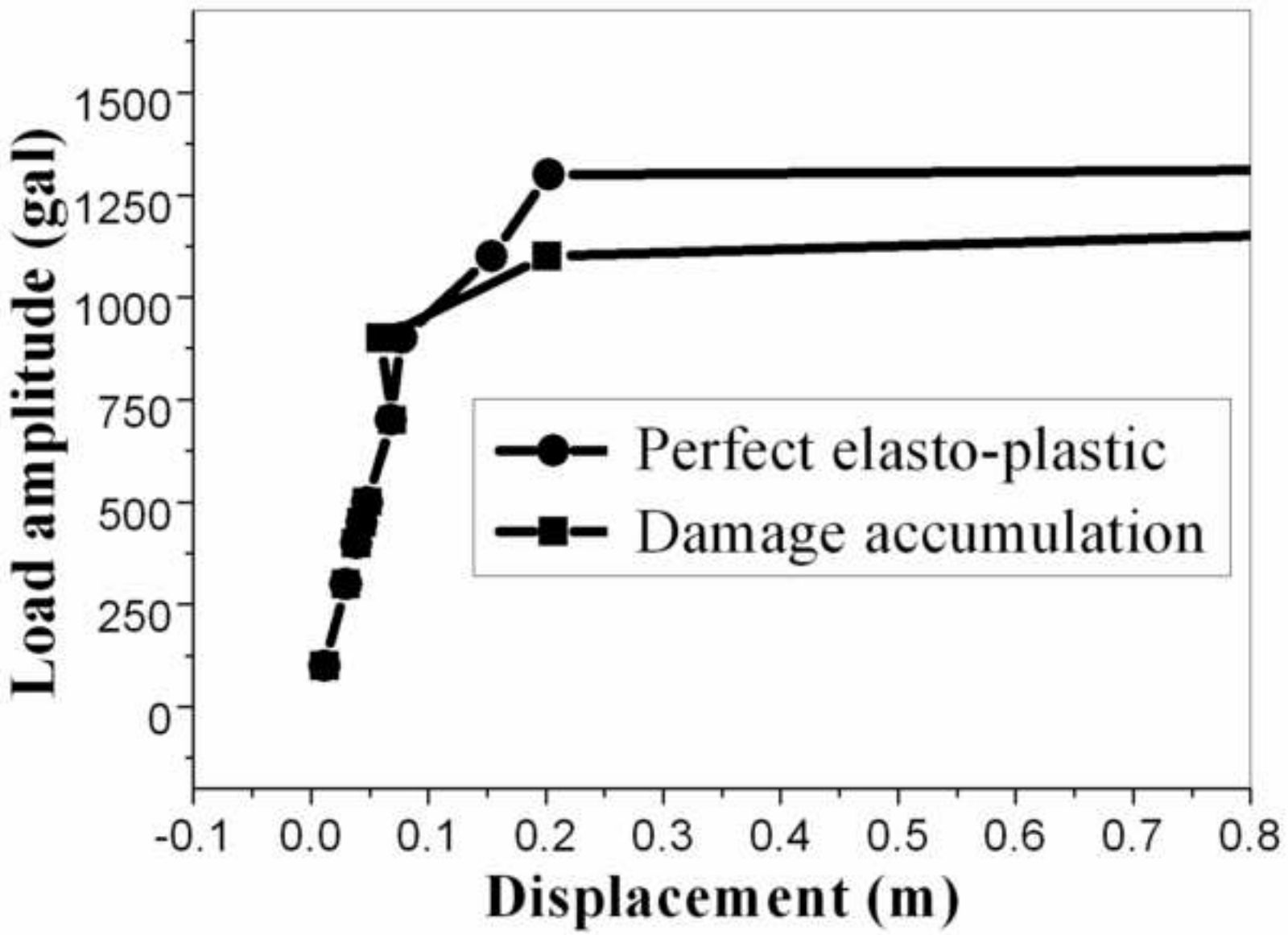

Journal of Structural Engineering. Submitted May 11, 2010; accepted February 10, 2011;
posted ahead of print February 12, 2011. doi:10.1061/(ASCE)ST.1943-541X.0000392

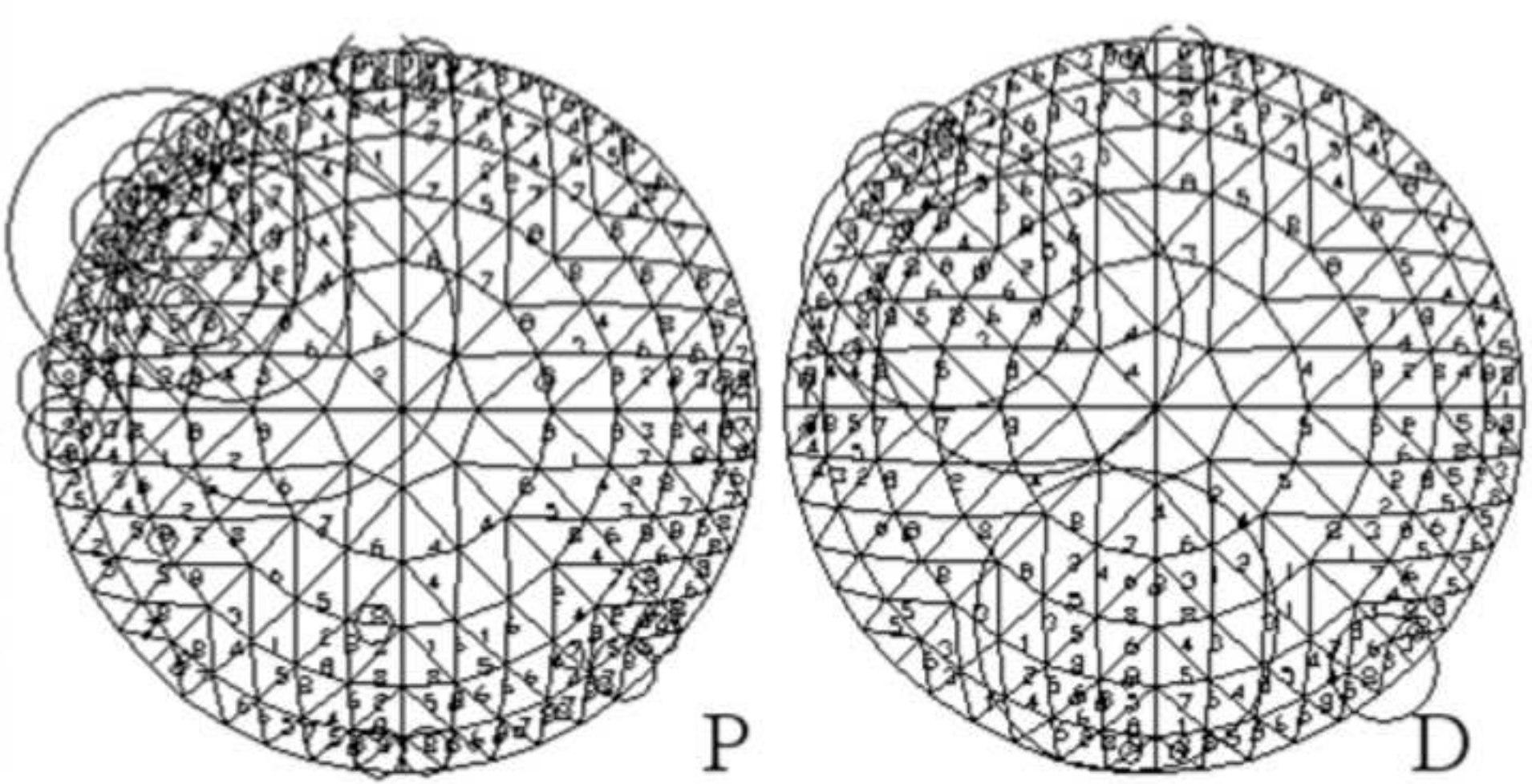

Journal of Structural Engineering. Submitted May 11, 2010; accepted February 10, 2011;
posted ahead of print February 12, 2011. doi:10.1061/(ASCE)ST.1943-541X.0000392

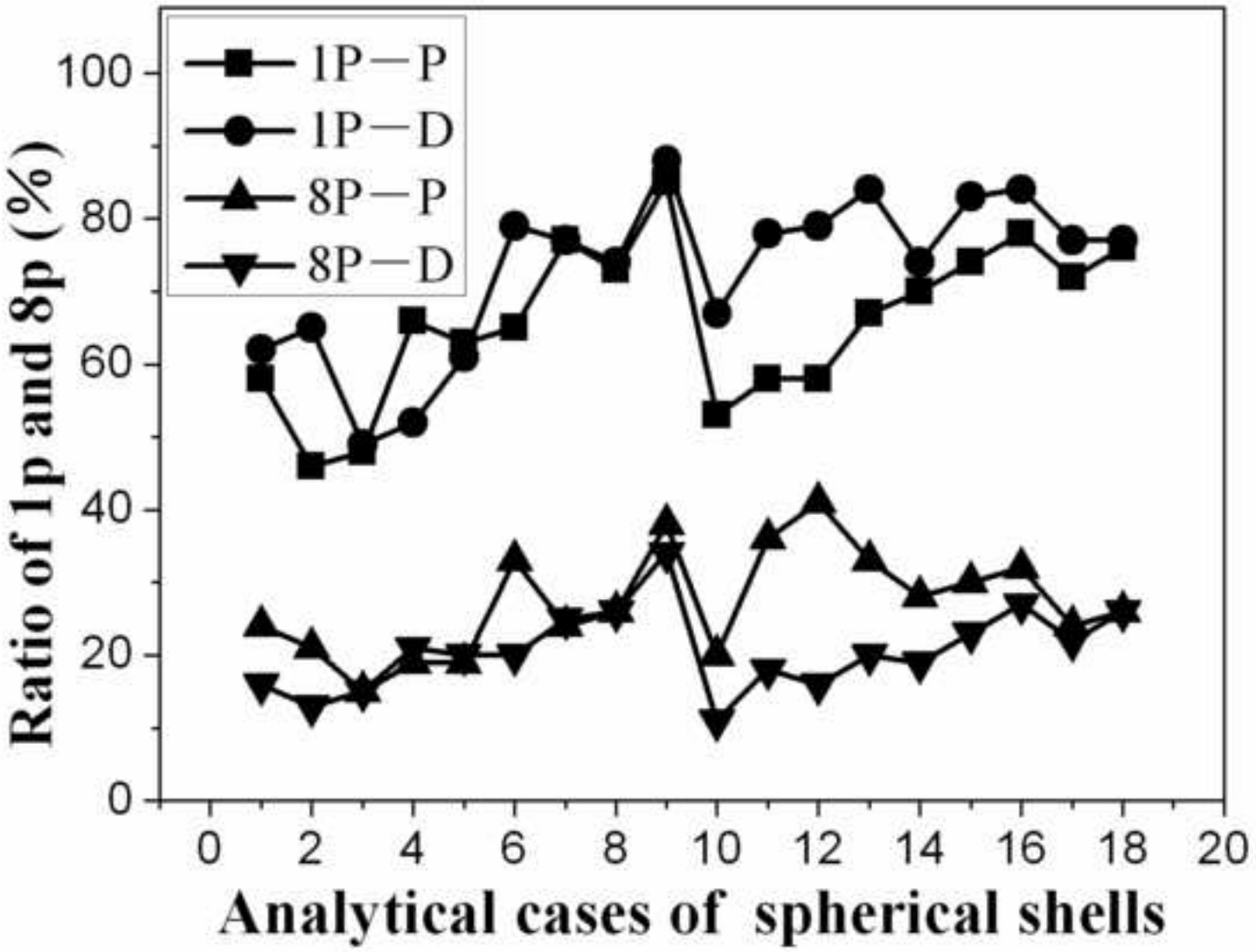

Journal of Structural Engineering. Submitted May 11, 2010; accepted February 10, 2011;
posted ahead of print February 12, 2011. doi:10.1061/(ASCE)ST.1943-541X.0000392

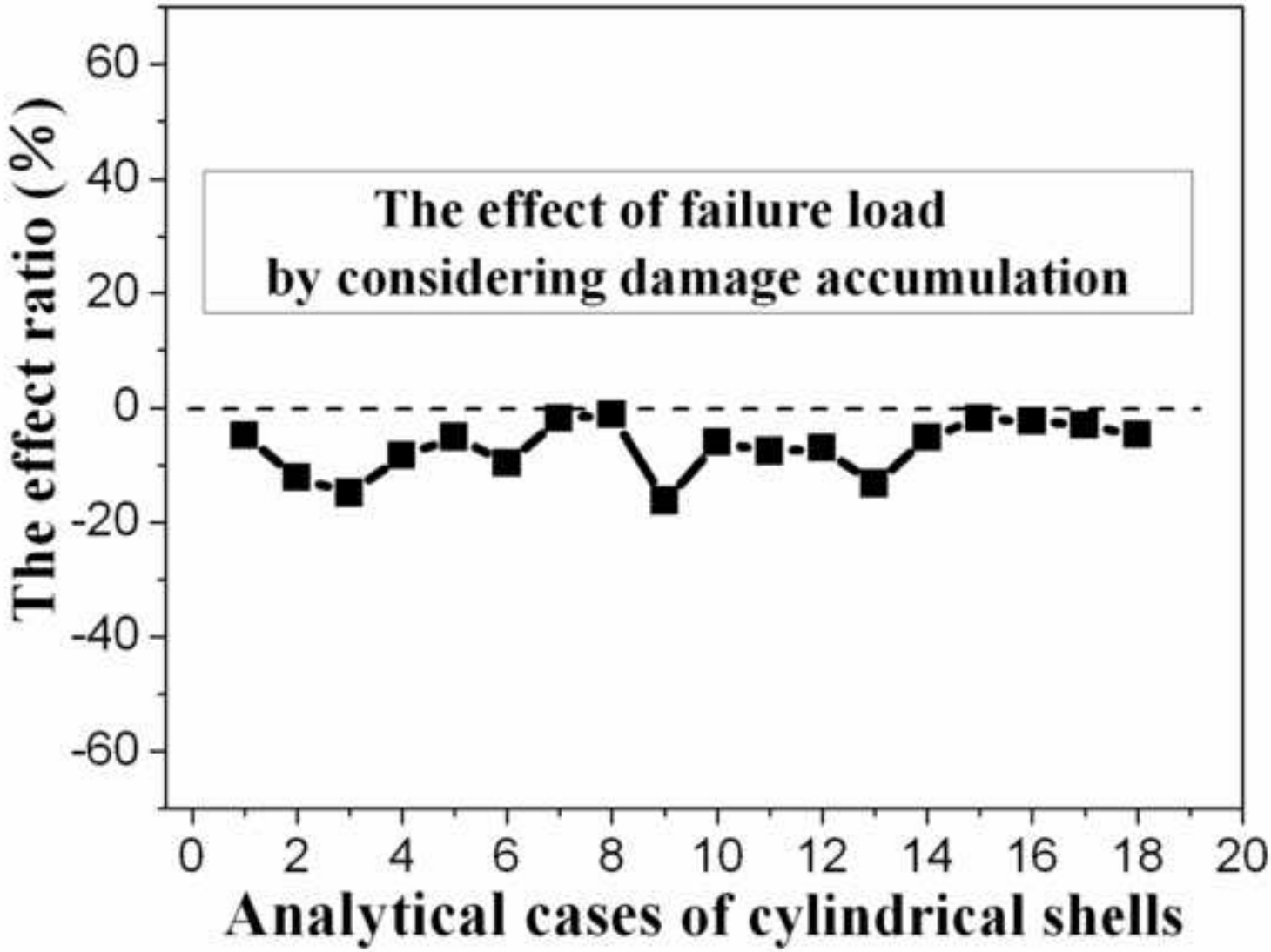

Journal of Structural Engineering. Submitted May 11, 2010; accepted February 10, 2011;
posted ahead of print February 12, 2011. doi:10.1061/(ASCE)ST.1943-541X.0000392

(a) Specimen (b) Specific explanation of loading setup (c) Three-direction loading

Fig.1 Specimen and loading setup

(a) Horizontal load arrangement (1=Specimen; 2=Hinge; 3=Load cell; 4=Hydraulic jack; 5=Hinged support; 6=LVDT)

(b) Loading in the axial (7=Central strut; 8= Free-movement plate; 9=Side bar; 10=Fixed plate; 11=Load cell; 12=Jack; 13=Top plate;

14=Specimen; 15=Steel ball) (c) Compression loading (d) Tensile loading

Fig.2 Details of the loading

(a) Load scheme 6 (b) Load scheme 7 (c) Load scheme 8 (d) Load scheme 9 (e) Load scheme 10

Fig.3 Load schemes of specimen

(a) Specimen S-21 (b) Specimen S-22 (c) Specimen S-23 (d) Specimen S-24 (e) Specimen S-25

Fig.4 Hysteretic curves and failure of specimens S-21 to S-25

(a) Hysteretic curves in x direction of S-23 (b) Hysteretic curves in y direction of S-23 (c) Hysteretic curves in z direction of S-28

(d) Hysteretic curves in x direction of S-28 (e) Hysteretic curves in y direction of S-28

Fig.5 Hysteretic curves of Specimens S-23 and S-28

(a) Schematic drawing of the rotation of steel box (b) Comparison curves of displacement in x direction (c) Comparison of curves of

displacement in y direction

Fig.6 Schematic drawing of the rotation of steel box and comparison curves of specimen S-23

(a) Schematic drawing of specimen in test (b) Comparison curves

Fig.7 Schematic drawing of specimen in test and comparison curves of x and y of Specimen S-23

Fig.8 The flow process of UMAT

Fig.9 Curves established using trial and error method (Hysteretic curves of Specimen S-12 when β =0.019 , ξ_1 =0.331 , ξ_2 =0.059)

(a) Comparison of curves in x direction of S-21 (b) Comparison of curves in y direction of S-21

(c)Comparison of curves in x direction of S-27 (d) Comparison of curves in axial direction of S-27

Journal of Structural Engineering. Submitted May 11, 2010; accepted February 10, 2011;
posted ahead of print February 12, 2011. doi:10.1061/(ASCE)ST.1943-541X.0000392

Fig.10 Simulation of specimens S-21 and S-27 validating the constitutive model

(a) The spherical shell (b) The cylindrical shell

Fig.11 The schematic drawing of the reticulated shells

Fig.12 Definition for different levels of development of plastic deformation on cross-section

(a) Yielded member ratio versus load magnitude (P-perfect elasto-plastic, D-damage accumulation)

(b) Maximum node displacement versus time (P-perfect elasto-plastic, D-damage accumulation)

(c) Maximum displacement versus load magnitude (d) Development of plastic deformation at failure

Fig.13 Analytical results of characteristic responses of the structure

(a) Ratio of 1p and 8p of yielded members (b) Failure load of cylindrical shells

Fig.14 The characteristic responses with and without considering damage accumulation (P - perfect elasto-plastic, D - damage accumulation)